SIRT1 regulates sphingolipid metabolism and neural differentiation of mouse embryonic stem cells through c-Myc-SMPDL3B

Wei Fan,[1] Shuang Tang, [1, 6] Xiaojuan Fan, [2] Yi Fang,[1] Xiaojiang Xu, [3] Leping Li, [4] Jian Xu, [5] Jian-Liang Li, [3] Zefeng Wang, [2, *] and Xiaoling Li [1, *]

[1]Signal Transduction Laboratory, National Institute of Environmental Health Sciences, Research Triangle Park, NC 27709, USA

[2]CAS Key Laboratory of Computational Biology, CAS-MPG Partner Institute for Computational Biology, Shanghai Institute of Nutrition and Health, Shanghai Institutes for Biological Sciences, University of Chinese Academy of Sciences, CAS Center for Excellence in Molecular Cell Science, Chinese Academy of Sciences, Shanghai 200031, China

[3]Integrative Bioinformatics Support Group, National Institute of Environmental Health Sciences, Research Triangle Park, NC 27709, USA

[4]Biostatistics & Computational Biology Branch, National Institute of Environmental Health Sciences, Research Triangle Park, NC 27709, USA

[5]Children's Medical Center Research Institute, Department of Pediatrics, Harold C. Simmons Comprehensive Cancer Center, and Hamon Center for Regenerative Science and Medicine, University of Texas Southwestern Medical Center, Dallas, TX 75390, USA.

[6]Current address: Cancer Institute and Department of Nuclear Medicine, Fudan University Shanghai Cancer Center, Shanghai 200032, China

* Correspondence: lix3@niehs.nih.gov (X. L.), wangzefeng@picb.ac.cn (Z. W.)

Short title: SIRT1 regulates sphingolipid metabolism

Key words: SIRT1; sphingomyelin degradation; embryonic stem cells; neural development; embryogenesis; c-Myc

Abstract

Sphingolipids are important structural components of cell membranes and prominent signaling molecules controlling cell growth, differentiation, and apoptosis. Sphingolipids are particularly abundant in the brain, and defects in sphingolipid degradation are associated with several human neurodegenerative diseases. However, molecular mechanisms governing sphingolipid metabolism remain unclear. Here we report that sphingolipid degradation is under transcriptional control of SIRT1, a highly conserved mammalian NAD^+-dependent protein deacetylase, in mouse embryonic stem cells (mESCs). Deletion of SIRT1 results in accumulation of sphingomyelin in mESCs, primarily due to reduction of SMPDL3B, a GPI-anchored plasma membrane bound sphingomyelin phosphodiesterase. Mechanistically, SIRT1 regulates transcription of *Smpdl3b* through c-Myc. Functionally, SIRT1 deficiency-induced accumulation of sphingomyelin increases membrane fluidity and impairs neural differentiation *in vitro* and *in vivo*. Our findings discover a key regulatory mechanism for sphingolipid homeostasis and neural differentiation, further imply that pharmacological manipulation of SIRT1-mediated sphingomyelin degradation might be beneficial for treatment of human neurological diseases.

Introduction

First isolated from brain extract in the 1880s, sphingolipid is a class of natural lipids containing a backbone of sphingoid base sphingosine (1-3). Sphingolipids not only are the structural components of cell membranes, but also act as signaling molecules to control various cellular events, including signal transduction, cell growth, differentiation, and apoptosis (4, 5). Particularly, sphingolipids are enriched in microdomains/lipid rafts, a liquid-ordered phase in plasma membrane, where sphingomyelin, glycosphingolipids and cholesterol form unique platforms for many different proteins that are important for nutrient transport, organelle contact, membrane trafficking, and homotypic fusion (6).

The homeostasis of sphingolipids is maintained by a highly coordinated metabolic network that links together various pathways with ceramide as a central node (Figure S1A). Firstly, ceramide can be *de novo* synthesized in endoplasmic reticulum (ER), starting from the condensation of serine and fatty acyl-CoA by serine palmitoyltransferase (SPT). Ceramide is then transported to the Golgi complex and further converted into more complex forms of sphingolipids, such as glycosphingolipids or sphingomyelin. Secondly, ceramide can be regenerated by hydrolysis of complex sphingolipids in the Golgi complex and plasma membrane, which is catalyzed by a class of specific hydrolases and phosphodiesterases. For example, regeneration of ceramide from sphingomyelin can be mediated by plasma membrane bound sphingomyelin phosphodiesterases (SMPDs), including SMPDL3B, a GPI-anchored lipid raft SMPD (7). By degrading sphingomyelin, SMPDL3B regulates plasma membrane fluidity, which in turn impacts TLR-mediated innate immunity in macrophages (7) and modulates insulin receptor signaling in podocytes (8). Sphingolipid metabolism is highly sensitive to environmental/nutritional perturbations. Sphingolipid biosynthesis and accumulation can be induced by high-fat diet (HFD) feeding in multiple tissues in mice (9). Sphingolipids are also accumulated during aging (10, 11), and caloric restriction, a dietary regimen known to extend life span and delay a number of

78 age-associated diseases, decreases sphingolipid accumulation by reducing the activity of
79 SPT (12). Dietary serine restriction also alters sphingolipid diversity and synthesis to
80 constrain tumor growth (13).

81 Disruption of sphingolipid homeostasis has been involved in the pathogenesis of
82 a number of human diseases, such as Niemann-Pick disease and neurodegenerative
83 Alzheimer's, Parkinson's, and Huntington's diseases. These human diseases are
84 generally the outcome of defect in enzymes that degrade the sphingolipids (14, 15). Such
85 degradation defect leads to accumulation of sphingolipids, which in turn dramatically alters
86 cellular membrane structure and signaling, thereby triggering various diseases.
87 Consequently, manipulation of one enzyme or metabolite in sphingolipid degradation
88 pathways may result in unexpected changes in cellular metabolic programs and related
89 cellular functions (14, 15). However, molecular mechanisms that regulate the expression
90 of these sphingolipid degrading enzymes remain unclear.

91 In the present study, we investigated the role of SIRT1 in regulation of sphingolipid
92 degradation in mouse embryonic stem cells (mESCs) and mouse embryos. SIRT1 is a
93 NAD^+-dependent protein deacetylase critical for multiple cellular processes, including
94 metabolism, inflammation, stress response, and stem cell functions (16-18). SIRT1 is also
95 a key regulator of animal development (19-21), and is particularly important in the central
96 nervous system. For instance, SIRT1 has a major influence on hypothalamic function, and
97 cell-type specific SIRT1 mutations result in defects in systemic energy metabolism,
98 circadian rhythm, and the lifespan of the animal (22-25). SIRT1 also modulates dendritic
99 and axonal growth (26, 27), and regulates synaptic plasticity and memory formation in
100 adult brain (28). Moreover, SIRT1 has been shown to ameliorate neurodegenerative
101 phenotypes in animal models of Alzheimer's, Parkinson's, and Huntington's disease
102 (reviewed in (29)). However, despite multiple mechanisms proposed for these critical roles
103 of SIRT1 in the brain, how SIRT1 regulates neural development and function remain

unclear. Through global metabolomics and cellular metabolic characterizations, we discovered that SIRT1 deficiency in mESCs results in abnormal accumulation of sphingolipids, primarily due to reduced degradation of these lipids. We further found that this abnormal accumulation of sphingolipids does not affect the maintenance of pluripotent mESCs, but delays their neural differentiation during *in vitro* neural differentiation and *in vivo* mouse embryogenesis. Moreover, we provide evidence that SIRT1 regulates sphingolipid metabolism through deacetylation of c-Myc transcription factor, which promotes the expression of SMPDL3B and subsequent sphingomyelin degradation in mESCs. Together, our study identifies the SIRT1-c-Myc axis as an important regulatory mechanism for cellular sphingolipid metabolism and neural differentiation.

Results

Deletion of SIRT1 in ESCs results in accumulation of sphingomyelin

During a large-scale unbiased metabolomic analysis of WT and SIRT1 KO mESCs cultured in a serum-containing M10 medium, we discovered that SIRT1 KO mESCs display altered lipid metabolism, particularly metabolites involved in sphingolipid metabolism (Figure 1A and Table S1), in addition to previously reported metabolic defects in methionine metabolism (30). Specifically, SIRT1 KO mESCs had a dramatic accumulation of sphingomyelin in both complete medium and a methionine restricted medium (Figure 1B, S1B, and Table S1). Moreover, deletion of SIRT1 in mel1 human ESCs by CRISPR/Cas9-mediated gene editing technology (Figure S1C) also led to accumulation of several types of sphingomyelin regardless of medium methionine contents (Table S2), indicating that SIRT1 regulates sphingolipid metabolism in ESCs independently of cellular methionine metabolism.

To confirm that deletion of SIRT1 indeed increases sphingomyelin contents in ESCs, we loaded WT and SIRT1 KO mESCs cultured in serum-free ESGRO medium with

a green-fluorescent dye labeled sphingomyelin, BODIPY FL-C5-sphingomyelin, for 30 min at 4 °C, then chased at 37 °C for 30 min. Both WT and SIRT1 KO mESCs were labeled with this green-fluorescent sphingomyelin (Figure 1C). However, SIRT1 KO mESCs had marked accumulation of BODIPY FL-C5-sphingomyelin inside cells, presumably in ER and Golgi, compared to WT mESCs. Quantitative FACS analysis showed that SIRT1 KO mESCs have about a 50% increase in cellular levels of BODIPY FL-C5-sphingomyelin compared to WT mESCs (Figure 1D). An enzyme-coupled colorimetric assay further revealed a ~60% increase of endogenous sphingomyelin in SIRT1 KO mESCs (Figure 1E). Interestingly, the accumulation of sphingomyelin was specific to mESCs, as SIRT1 KO MEFs had a comparable staining intensity of BODIPY FL-C5-sphingomyelin as WT MEFs (Figure S1D). Additionally, SIRT1 KO mESCs had a similar staining intensity of BODIPY FL-N6-Ceramide compared to WT mESCs (Figure S1E), suggesting that accumulation of sphingolipids in SIRT1 KO mESCs is specific to sphingomyelin.

SIRT1 KO mESCs in above analyses were previously generated in R1 mES cell line using traditional gene targeting technology (19). To further confirm our observation that SIRT1 deficiency in mESCs induces accumulation of sphingomyelin, we deleted *Sirt1* gene in another widely-used full pluripotent mES cell line, E14 cells (31), by CRISPR/Cas9-mediated gene editing technology (Figure 1F). Consistent with observations in SIRT1 KO mESCs, these SIRT1 KO E14 mESC clones also had an enhanced staining of BODIPY FL-C5-sphingomyelin when analyzed by confocal fluorescence imaging (Figure 1G) and by quantitative FACS analysis (Figure 1H). Taken together, our results indicate that deletion of SIRT1 in ESCs results in accumulation of sphingomyelin in independent ES cell lines.

Deletion of SIRT1 induces accumulation of sphingomyelin through SMPDL3B

Cellular levels of sphingomyelin are regulated by a tight balance between their synthesis and breakdown, which are mediated by activities of sphingomyelin synthases (SGMSs) and sphingomyelin phosphodiesterases (SMPDs), respectively (Figure S1A). Many of these enzymes were highly expressed in mESCs (Figure S2A and S2B). To better understand how SIRT1 deficiency in mESCs leads to sphingomyelin accumulation, we surveyed the expression levels of these enzymes in WT and SIRT1 KO mESCs. SIRT1 KO mESCs had significantly reduced expression of a sphingomyelin synthase *Sgms2* (Figure 2A and S2B), and a dramatic reduction of a sphingomyelin phosphodiesterase SMPDL3B, one of most highly expressed SMPDs in mESCs (Figure S2A), in both ESGRO and M10 media (Figure 2A-2C). Since sphingomyelin was accumulated in SIRT1 KO mESCs, we focused on the reduction of *Smpdl3b*. As shown in Figure 2D, the reduced expression of SMPDL3B in SIRT1 KO mESCs was coupled with a decreased rate to clear away preloaded BODIPY FL-C5-sphingomyelin in a time-lapse video analysis, suggesting that reduction of SMPDL3B-mediated sphingomyelin degradation may be responsible for accumulation of sphingomyelin observed in SIRT1 KO mESCs.

To test this possibility, we manipulated the levels of SMPDL3B in WT and SIRT1 KO mESCs and analyzed their impacts on cellular levels of sphingomyelin. Stable overexpression of SMPDL3B significantly reduced accumulation of BODIPY FL-C5-sphingomyelin in SIRT1 KO but not WT mESCs when cells were cultured in serum-containing M10 medium (Figure 3A-3C). In serum-free ESGRO medium, overexpression of SMPDL3B reduced accumulation of BODIPY FL-C5-sphingomyelin and endogenous sphingomyelin in both WT and SIRT1 KO mESCs (Figure 3D-3F). These results indicate that SMPDL3B is capable of removing sphingomyelin in mESCs, particularly in SIRT1 KO mESCs. Conversely, shRNA-mediated stable knockdown of SMPDL3B (Figure 3G) enhanced the accumulation of BODIPY FL-C5-sphingomyelin (Figure 3H and 3I) and endogenous sphingomyelin (Figure 3J) in WT mESCs but not further in SIRT1 KO mESCs,

indicating that accumulation of sphingomyelin observed in SIRT1 KO mESCs is primarily due to reduced expression of SMPDL3B.

SIRT1 promotes transcription of *Smpdl3b* through c-Myc

As an NAD^+-dependent protein deacetylase that deacetylates histones, transcription factors, cofactors, as well as splicing factors, SIRT1 has been shown to modulate gene expression at multiple levels. We confirmed that SIRT1 indeed regulates the expression of *Smpdl3b* and sphingomyelin degradation through its catalytic activity, as a SIRT1 catalytic inactive mutant (H355Y, HY) failed to rescue defective *Smpdl3b* expression and reduce BODIPY FL-C5-sphingomyelin accumulation in SIRT1 KO mESCs compared to WT SIRT1 protein (Figure 4). When interrogated each step along the expression of *Smpdl3b* gene in SIRT1 KO mESCs, we found that qPCR primers designed to amplify different segments of mature *Smpdl3b* mRNA all detected a reduced abundance of the full-length mature *Smpdl3b* mRNA upon SIRT1 deletion in mESCs (Figure S3A and S3B). Moreover, the abundance of *Smpdl3b* mRNA was reduced in both nuclear and cytosolic fractions in SIRT1 KO mESCs (Figure S3C). Northern blotting analysis using random probes generated from full-length *Smpdl3b* cDNA further showed that deletion of SIRT1 in mESCs reduces the abundance of full-length *Smpdl3b* mRNA without detectable accumulation of other minor isoforms (Figure S3D). Finally, RNA-seq analysis of total Ribo-minus RNA (total RNA after depletion of ribosomal RNAs) revealed that the abundance of RNA species from both exonic and intronic regions of *Smpdl3b* gene were reduced in SIRT1 KO mESCs (Figure S3E and Table S3), and no defective splicing of *Smpdl3b* pre-mRNA was detected in these cells (not shown). All these observations strongly suggest that the reduction of SMDPL3B expression in SIRT1 KO mESCs is due to defective transcription of *Smpdl3b* gene. In support of this notion, SIRT1 KO mESCs had a drastic depletion of Pol II near the TSS of *Smpdl3b* gene, along with decreased

association of activation mark H3K4me3 yet increased association of repression mark H3K27me3 (Figure 5A), indicative of a strong attenuation of transcriptional activation of *Smpdl3b* gene in SIRT1 KO mESCs.

Sequence analysis of the TSS region revealed multiple potential transcription factors (TFs) that may target *Smpdl3b* gene, including two known SIRT1 deacetylation substrates c-Myc and N-Myc (30, 32) (Figure 5B). To determine the promoter region(s) and associated TF(s) that are responsible for the transcription suppression of *Smpdl3b* gene in SIRT1 KO mESCs, we designed small gRNAs (sgRNAs) to target different potential TF loci along the *Smpdl3b* promoter (Figure S4A, top), then analyzed their impacts on the expression of *Smpdl3b* after transfecting into WT and SIRT1 KO mESCs generated from a mouse ES cell line stably expressing a dox-inducible dCas9 and BirA-V5 (dCas9 mESCs, Figure S4B) (33). It has been demonstrated that transfected sgRNAs in these cells are able to guide the deactivated Cas9 (dCas9) to bind to their targeting loci without further cleavage, resulting in altered transcription of the target gene (33). Compared to control Gal4 sgRNA and other sgRNAs, a sgRNA targeting a locus near 528 bp downstream of the TSS of *Smpdl3b* gene rescued the defective expression of *Smpdl3b* mRNA in SIRT1 KO dCas9mESCs (Figure 5C). Further bioinformatic analysis showed that this locus is overlapped with previously mapped binding regions of two TFs, c-Myc and EZH2 (Figure S4A, bottom).

c-Myc is a known SIRT1 deacetylation substrate, and deacetylation of c-Myc by SIRT1 has been reported to increase its stability and activity (32). We have previously shown that c-Myc is hyperacetylated but unstable in SIRT1 KO mESCs, which reduces its binding to target promoters thereby decreasing their transcription (30). The association of c-Myc protein to the promoter of *Smpdl3b* gene was indeed significantly reduced in SIRT1 KO mESCs by a ChIP-qPCR assay (Figure 5A, c-Myc). Moreover, inhibition of c-Myc activity by 10058-F4 (34) (Figure 5D) or knocking down c-Myc with siRNAs (Figure 5E)

significantly reduced the mRNA abundance of *Smpdl3b* in WT mESCs but not or to a less extend in SIRT1 KO mESCs, indicating that c-Myc is a key transcription factor in SIRT1-mediated regulation of *Smpdl3b*. Furthermore, SIRT1 promoted the transcription of *Smpdl3b* in part through deacetylating c-Myc, as a c-Myc mutant with its major acetylation site mutated to R to mimic deacetylated c-Myc (K323R, KR), partially rescued the expression of *Smpdl3b* in SIRT1 KO mESCs compared to empty vector (V), WT c-Myc, and a c-Myc mutant with its major acetylation site mutated Q to mimic acetylated c-Myc (K323Q, KQ) (Figure S5C and Figure 5F). Finally, a *Smpdl3b* promoter luciferase reporter containing a mutant c-Myc binding site (E-box) displayed a dramatically reduced activity in mESCs compared to a WT *Smpdl3b* promoter luciferase reporter (Figure 5G, *pGL3-Smpdl3b E-box Mut* vs *pGL3-Smpdl3b WT* in WT mESCs). Additionally, this mutant luciferase reporter had a comparable low activity in SIRT1 KO mESCs vs WT mESCs, further suggesting that the differential expression levels of *Smpdl3b* in WT and SIRT1 KO mESCs is mediated by c-Myc.

EZH2, an H3K27me3 methyltransferase and the functional enzymatic component of the Polycomb Repressive Complex 2 (PRC2), is also a deacetylation substrate of SIRT1 (35). Deacetylation of K348 of EZH2 by SIRT1 has been reported to reduce its stability and activity (35), which is consistent with our current observations that deletion of SIRT1 in mESCs significantly increased the occupancy of EZH2 and H3K27me3 on the promoter of *Smpdl3b* gene (Figure 4A, EZH2, H3K27me3). However, in contrast to c-Myc, neither inhibition of EZH2 activity by its inhibitor EPZ6438 (Figure S4D) nor knockdown of EZH2 by siRNAs (Figure S4E-S4G) significantly affected the expression of *Smpdl3b* in mESCs, particularly in SIRT1 KO mESCs, indicating that blocking EZH2-catalyzed H3K27 trimethylation alone is not sufficient to rescue SIRT1 deficiency-induced transcriptional suppression of *Smpdl3b* in mESCs. Collectively, our data demonstrate that SIRT1 activates the expression of *Smpdl3b* in mESCs primarily through deacetylation of c-Myc.

SIRT1-regulated sphingolipid metabolism affects *in vitro* neural differentiation

SMPDL3B-catalyzed sphingomyelin degradation has been shown to reduce plasma membrane fluidity (7). As expected from their reduced expression of SMPDL3B, SIRT1 KO mESCs had a reduced fraction of ordered structures (thereby increased membrane fluidity) compared to WT mESCs when probed with Di-4-ANEPPDHQ, an electrical potential sensitive fluorescent dye for detection of microdomains and (dis)ordered membrane in live cells, (Figure 6A, vehicle). Treatment with methyl-β-cyclodextrin (MβCD), a cholesterol-extracting agent, further decreased the membrane order, particularly in SIRT1 KO mESCs (Figure 6A, MβCD). In line with this observation, pathways involved in membrane function and signaling were among the most significantly disrupted GO terms in SIRT1 KO mESCs when compared with WT mESCs in our Ribo-minus RNA-seq dataset (Figure S5).

Sphingolipids are bioactive lipids important for stem cell survival and differentiation (36, 37). Since we previously observed that SIRT1 KO mESCs have a compromised pluripotency (30), we investigated whether sphingomyelin accumulation in SIRT1 KO mESCs is responsible for their reduced pluripotency. Compared to WT mESCs, SIRT1 KO mESCs had a reduced staining intensity of Alkaline Phosphatase (AP), a marker of undifferentiated ESCs (Figure 6B), along with decreased expression of OCT3/4 and Nanog, two pluripotent stem cell markers, and increased expression of Nestin, a neuroectodermal stem cell (NSC) marker (Figure 6C). However, sphingomyelin treatment did not consistently affect the AP staining intensity (Figure 6B) nor induced any significantly changes on the expression of pluripotency markers in either WT or SIRT1 KO mESCs (Figure 6C, OCT3/4 and Nanog). In contrast, sphingomyelin dose-dependently increased the expression of Nestin, a neuroectodermal stem cell (NSG) marker that was

induced in SIRT1 KO mESCs, in WT mESCs (Figure 6C, Nestin), suggesting that sphingomyelin accumulation may interfere neural differentiation in SIRT1 KO mESCs instead of their pluripotency.

Consistent with this observation, during a 4-week *in vitro* neural differentiation of mESCs (Figure 7A) (38, 39), the mRNA levels of *Sirt1* were significantly reduced in WT E14 mESCs, along with dramatic decrease of *Nanog* and *Oct4* and massive induction of several NSC and neural differentiation factors, such as *Sox3*, *Nestin*, *Notch3*, and *Tau* (Figure 7B, WT). However, both the reduction of pluripotency markers and the induction of NSC/neural differentiation factors were significantly blunted when SIRT1 was deleted in E14 mESCs (Figure 7B, KO), indicating that SIRT1 deficiency impairs *in vitro* neural differentiation of these cells. Further cellular and morphological analyses by immunofluorescence staining of progenitor and neuronal markers showed that progenitors and neurons differentiated from WT E14 mESCs have high expression of marker proteins and typical mature neuronal morphology, including elongated axons and dendrites, after 4-week differentiation (Figure 7C, WT). Progenitors and neurons differentiated from SIRT1 KO E14 mESCs, on the other hand, had low levels of these markers and lacked typical neuronal morphology (Figure 7C, KO). Additionally, SIRT1 KO mESCs also displayed defective neural differentiation after *in vitro* differentiation (Figure 7D), indicating that SIRT1 deficiency in mESCs impairs neural differentiation *in vitro* in a cell line independent manner.

To validate that defective neural differentiation of SIRT1 KO mESCs is related to its accumulation of sphingomyelin, we analyzed whether adding back SMPDL3B in these cells will rescue their neural differentiation defects. Morphologically, putting back SMPDL3B into SIRT1 KO mESCs increased neurons with elongated axons and dendrites (Figure 8A and 8B, SIRT1 KO SMPDL3B), which was associated with increased expression of several progenitor and neuronal markers when analyzed by

immunofluorescence staining (Figure 8B, SIRT1 KO SMPDL3B) or by qPCR (Figure 8C, SIRT1 KO SMPDL3B). Overexpression of SMPDL3B in WT mESCs, however, disrupted the expression of progenitor markers and morphology of neurons (Figure 8B, SIRT1 WT SMPDL3B), suggesting that a balanced sphingomyelin degradation is required to maintain normal neural differentiation. Quantification of the fraction of cells positive of several neural markers by FACS analysis further confirmed that putting back SMPDL3B partially rescues the neural differentiation defects in SIRT1 KO mESCs, whereas overexpression of SMPDL3B inhibits normal neural differentiation in WT mESCs (Figure 8D). Conversely, *in vitro* neural differentiation of WT and SIRT1 KO mESCs with or without stable knockdown of SMPDL3B revealed that reduction of this enzyme disrupts neural differentiation in both WT and SIRT1 KO mESCs (Figure 8E), indicative the importance of this enzyme in normal neural differentiation. Finally, putting back WT SIRT1 protein into SIRT1 KO mESCs rescued expression of progenitor marker SOX1 and NSC marker Nestin as well as neuronal morphology after *in vitro* neural differentiation (Figure 8F, SIRT1 KO-WT). In contrast, putting back a catalytic inactive SIRT1 mutant failed to restore marker protein expression and/or neuronal morphology (Figure 8F, SIRT1 KO-HY), confirming that the neural differentiation defects observed in SIRT1 KO mESCs are primarily due to a lack of SIRT1 deacetylase activity. Taken together, our observations indicate that SIRT1-mediated transcription of *Smpdl3b* and sphingolipid degradation influence neural differentiation *in vitro*.

Maternal high-fat diet feeding induces accumulation of sphingomyelin and impairs neural development in SIRT1 deficient embryos

To assess the importance of sphingolipid metabolism in SIRT1-regulated neural differentiation *in vivo*, we investigated whether embryonic SIRT1 deficiency is associated with altered sphingomyelin accumulation and neural differentiation in mice. Consistent

with our previous observations (30), systemic deletion of SIRT1 in C57BL/6J mice leads to intrauterine growth retardation when dams were fed on a regular chow diet (containing 4% fat) (Figure 9A, chow). The mRNA levels of *Smpdl3b* were significantly reduced in the brain of SIRT1 KO E18.5 embryos (Figure 9B). However, these embryos did not display any detectable defects in brain sphingomyelin levels, nor in expression of a number of neural progenitor and neuron markers (Figure 9C and 9D, chow) despite reported developmental defects in other systems(19-21). Since high-fat diet (HFD) feeding has been shown to induce sphingolipid biosynthesis and turnover of sphingolipids in multiple tissues (9), we tested whether maternal HFD feeding could induce sphingomyelin accumulation and disrupt neural development in SIRT1 KO embryos. Intriguingly, maternal feeding of an HFD diet containing 36% fat for 4-8 weeks before breeding significantly reduced intrauterine growth of embryos, particularly on SIRT1 KO embryos, at E18.5 (Figure 9A, HFD). Maternal HFD feeding also elevated sphingomyelin contents in all tested regions of brain in SIRT1 KO but not WT E18.5 embryos (Figure 9C, HFD). These maternal HFD feeding-induced gross and metabolic alterations were associated with reduced expression of many intermediate progenitor and mature neuron markers (Figure 9D, HFD) without significant changes on early stage neuroepithelial cell markers and oligodendrocyte marker (not shown), suggesting that SIRT1 deficiency-induces sphingomyelin accumulation specifically delays neuron maturation in mouse embryos.

Discussion

Highly enriched in the nervous system, sphingolipids are important for the development and maintenance of the functional integrity of the nervous system (40, 41). Perturbations of the sphingolipid metabolism has been shown to rearrange the plasma membrane, resulting in development of various human diseases, particularly neurological diseases (42). However, despite these diverse biological functions, the transcriptional regulation of

362 sphingolipid metabolism is largely unknown. In the present study, we show that cellular
363 sphingomyelin degradation is under transcriptional control of SIRT1, an important cellular
364 metabolic sensor. We provide evidence that the SIRT1-Myc axis is vital for transcriptional
365 activation of SMPDL3B, a major GPI-anchored plasma membrane bound sphingomyelin
366 phosphodiesterase in mESCs. This transcriptional regulation directly impacts cellular
367 levels of sphingomyelin and membrane fluidity, and is important in regulation of neural
368 differentiation in response to developmental signals (Figure 9E). Our findings therefore
369 identify a unique genetic regulatory pathway for sphingolipid homeostasis. Given the high
370 sensitivity of SIRT1 to nutritional and environmental perturbations (e.g. activation upon
371 caloric restriction and repression after HFD feeding or during aging (43, 44), our study
372 further suggests that SIRT1-Myc-regulatetd sphingolipid degradation may be an important
373 element in mediating reported environmental influence on sphingolipid metabolism (9-12).
374 It will be of great interest to test this possibility in future studies.

375 As the most conserved mammalian NAD^+-dependent protein deacetylase, SIRT1
376 has a number of important functions in the brain, including regulation of late stage of neural
377 development and protection against a number of neurodegenerative diseases (29). In
378 particular, SIRT1 has been shown to modulate the neural and glial specification of neural
379 precursors (45, 46) and repress low glucose induced proliferation and neurogenesis of
380 neural stem and progenitor cells (NSCs) *in vitro* (47). Our observations in the present
381 study demonstrate that SIRT1 is also a key metabolic regulator for the differentiation of
382 neural progenitors/NSCs from ESCs. Our results show that SIRT1 is highly expressed in
383 mESCs cells (Figure 7B), where it functions to promote c-Myc-mediated transcriptional
384 activation of SMPDL3B and sphingomyelin degradation (Figure 1-4). This action of SIRT1
385 appears to have minimal impacts on the pluripotency of mESCs (Figure 6B and 6C), but
386 instead is important for maintenance of a proper membrane fluidity for normal neural
387 differentiation in response to nutritional/developmental cues (Figure 9E). Thus, by

388 interacting with different protein factors, SIRT1 is important for neural differentiation and
389 development at multiple stages.

390 Our observations that *Smpdl3b* promoter is targeted by both c-Myc and EZH2,
391 consequently with "co-localization" of antagonistic epigenetic marks H3K4me3 and
392 H3K27me3 at the same locus near its TSS (Figure 4A and S5A), suggest that *Smpdl3b* in
393 mESCs might be a bivalent promoter-associated gene (48-50). The bivalent chromatin
394 domains in ESCs often mark lineage regulatory genes, and it has been proposed that
395 bivalent domains might repress lineage control genes by H3K27me3 during pluripotency
396 while keeping them poised for activation upon differentiation with H3K4me3 (50).
397 Interestingly, the bivalent chromatin domain on *Smpdl3b* appears to keep it active in
398 mESCs while poising it to be repressed upon differentiation. Moreover, while long-
399 recognized as a transcription repressor through deacetylation of histones, SIRT1 plays
400 an active role in remodeling this bivalent domain by stabilizing c-Myc while restricting
401 EZH2-induced H3K27me3 in mESCs (Figure 9E). Our present study reveals that this
402 SIRT1/c-Myc/EZH2-regulated bivalent domain remodeling enables swift membrane
403 remodeling in response to developmental signals, allowing more efficient and
404 synchronous neural differentiation. Premature disruption of this chromatin remodeling
405 complex in mESCs alters membrane fluidity (Figure 5A), which may in turn affect
406 developmental signaling transduction (e.g. insulin, bFGF) and impair neural differentiation.
407 Future studies will be needed to elucidate the general role of this bivalent chromatin switch
408 in regulation of pluripotency vs lineage genes, as well as in process of somatic cell
409 reprogramming and/or transformation.

410 The transcriptional regulation of sphingolipid metabolism and neural differentiation
411 by the SIRT1-Myc axis in mESCs revealed in our present study is very intriguing, as we
412 have previously reported that the same regulatory axis is key for methionine metabolism
413 and maintenance of pluripotency in mESCs (30). While our data show that accumulation

of sphingomyelin in SIRT1 KO mESCs is independently of methionine metabolism (Figure S1B and Table S1), additional studies are needed to assess how the SIRT1-Myc regulatory axis coordinates diverse metabolic processes to shape stem cell fates in response to different environmental signals. It is also worth noting that SIRT1 KO mESCs have additional lipid metabolic defects, including depletion of monoacyglycerols, accumulation of plasmalogens, acetylcholine, and monohydroxy fatty acids, and altered phospholipids, regardless of medium methionine concentrations (Figure S1B and Table S1). It will be of importance to evaluate the contribution of these lipid metabolic defects to the observed hypersensitivity of SIRT1 KO embryos to maternal HFD feeding-induced intrauterine growth retardation (Figure 7A) in future studies.

Our study has a number of important implications. Firstly, the previously uncharacterized transcriptional regulation of SIRT1 on sphingomyelin degradation directly links cellular levels of sphingomyelin and membrane fluidity with cellular energy status, and provides a possible molecular mechanism for the beneficial impacts of SIRT1 small molecule activators and/or NAD^+-boosting dietary supplements on human neurodegenerative diseases. Secondly, given the prevalence of obesity and metabolic syndrome in the reproductive population in modern society, the hypersensitivity of SIRT1 KO embryos to maternal HFD feeding-induced intrauterine growth retardation and neurodevelopmental defects suggests that pharmacological activation of SIRT1 by small molecule activators and/or NAD^+-boosting dietary supplements might be able to attenuate maternal obesity-associated neonatal complications and defective childhood neurodevelopment (51-53).

In summary, our study uncovers a SIRT1-Myc-mediated transcriptional regulation of sphingomyelin degradation that modulates neural differentiation of ESCs. This finding highlights the importance of SIRT1 and its regulation in mESC differentiation and embryonic development, and may have important implications in potential therapeutic

strategies again human neurodegenerative diseases and/or maternal obesity-induced adverse developmental outcomes.

Materials and Methods

Mammalian cell lines

WT ad SIRT1 KO mESCs generated in R1 mESC line have been reported previously (17, 19). WT and SIRT1 KO E14 mESCs were generated by CRISPR/Cas9 mediated gene editing technology using lentivirus carrying either all-in-one empty vector pCRISPR-CG01 vector or pCRISPR-CG01 containing different sgRNAs targeting mouse *Sirt1* gene (GeneCopoeia). Stable single colonies were picked up and screened with immunoblotting assay using anti-SIRT1 antibodies. Three independent WT and SIRT1 KO E14 mESCs were used for the experiments to minimize the potential off-target effects of each individual line. mESCs stably transfected with pEF1α-FB-dCas9-puro(Addgene #100547) and pEF1α-BirA-V5-neo (Addgene #100548) vectors (dCas9 mESCs) are described previously (33). WT and SIRT1 KO dCas9 mESCs were generated by a similar strategy as WT and SIRT1 KO E14 mESCs. Different sgRNA sequences targeting promoter region of Smpdl3b (Table S4) were cloned into plasmid pSLQ1651-sgRNA(F+E)-sgGal4 (Addgene #100549) and then were packed into lentivirus. The WT and SIRT1 KO dCas9 mESCs were infected with those lentiviruses to deliver sgRNA into cells, by which the dCas9 was able to be guided to bind on promotor region of Smpdl3b and interfere its functions.

WT and SIRT1 KO mESCs with stable Smpdl3b knockdown were generated by infecting WT and SIRT1 KO mESCs with lentivirus containing vector pLKO.1 or constructs expressing shRNAs against Smpdl3b (B11, B12, and C1) (Sigma). WT and SIRT1 KO mESCs with stable overexpression of SMPDL3B were generated with lentivirus carrying vector Plenti-III-ef1α (Abm) or constructs expressing the full-length SMPDL3B protein. The expression of SMPDL3B in these cells was analyzed by immunoblotting.

WT and SIRT1 KO mESCs with stable overexpression of WT or a catalytic inactive H355Y mutant (HY) were generated using lentivirus carrying empty vector Plenti-III-ef1α (Abm) or constructs expressing the full-length WT or HY SIRT1 proteins.

To knockdown the Ezh2 and C-Myc gene expression, WT and Sirt1 KO mESCs were transfected with siRNA against mouse Ezh2 (Thermofisher, 4390771-s65775; siNeg: 4390843) and c-Myc (Santa Cruz sc-29227; siNeg: siRNA-A sc-37007), with Lipofectamine RNAiMAX (ThermoFisher Scientific). The knockdown of genes expression was evaluated by Quantitative real-time PCR 48 hours after transfection.

All mouse stem cells were maintained on gelatin-coated plates in the ESGRO Complete Clonal Grade Medium (Millipore), and then cultured in the M10 medium (High glucose DMEM, 10% ES cell FBS, 2 mM L-glutamine, 1 mM sodium pyruvate, 0.1 mM nonessential amino acids, 10 μM 2-mercaptoethanol, and 500 units/ml leukocyte inhibitory factor) for some experiments.

WT and SIRT1 KO mel1 hESCs were generated by CRISPR/Cas9 mediated gene editing technology using a plasmid containing Cas9, gRNA (AGAGATGGCTGGAATTGTCC (- strand)) and a GFP indicator. The GFP positive cells were purified by flow cytometry, and were either grown on 10-cm dishes with a serial dilution, or in the 96-well plates at a density of 1 cell/well. Single colonies were picked up and subjected to immunofluorescence assay with anti-SIRT1 antibodies. The cell colonies without SIRT1 staining were sequenced to confirm the mutation. Three independent SIRT1 KO mel1 lines were used for the experiments to minimize the potential offtarget effects of each individual line.

Mouse models

Whole body SIRT1 knockout, heterozygote and their age-matched littermate WT mice on the C57BL/6J background have been reported before (17). They were housed in

individualized ventilated cages (Techniplast, Exton, PA) with a combination of autoclaved nesting material (Nestlet, Ancare Corp., Bellmore, NY and Crink-l'Nest, The Andersons, Inc., Maumee, OH) and housed on hardwood bedding (Sani-chips, PJ Murphy, Montville, NJ). Mice were maintained on a 12:12-h light:dark cycle at 22±0.5 °C and relative humidity of 40% to 60%. Mice were provided ad libitum autoclaved rodent diet (NIH31, Harlan Laboratories, Madison, WI) and deionized water treated by reverse osmosis. Mice were negative for mouse hepatitis virus, Sendai virus, pneumonia virus of mice, mouse parvovirus 1 and 2, epizootic diarrhea of infant mice, mouse norovirus, *Mycoplasma pulmonis, Helicobacter* spp., and endo- and ectoparasites upon receipt and no pathogens were detected in sentinel mice during this study.

Mice were randomly assigned to experimental groups after they were allowed to acclimate for at least one week prior to experiments.

Metabolomic analysis

WT and SIRT1 KO mESCs were cultured in the complete M10 medium containing 200 μM methionine or methionine restricted M10 medium containing 6 μM methionine for 6 hours (n=5 biological replicates). WT and SIRT1 KO mel1 hESCs were cultured in serum-free TeSR-E8 medium containing 116 μM methionine or a methionine restricted medium containing 6 μM methionine for 6 hours on Matrigel (n=4 biological replicates). Cells were then harvested and profiled by metabolomics analysis as previously described (30). Specifically, about 100 μl of packed cell pellet per sample were submitted to Metabolon, Inc. (Durham, NC, USA), where the relative amounts of small molecular metabolites were determined using four platforms of Ultrahigh Performance Liquid Chromatography-Tandem Mass Spectroscopy (UPLC-MS/MS) as previously described (55). All methods utilized a Waters ACQUITY UPLC and a Thermo Scientific Q-Exactive high

resolution/accurate mass spectrometer interfaced with a heated electrospray ionization (HESI-II) source and Orbitrap mass analyzer operated at 35,000 mass resolution. Raw data collected from above four analyses were managed by the Metabolon Laboratory Information Management System (LIMS), extracted, peak-identified and QC processed using Metabolon's hardware and software. The hardware and software foundations for these informatics components were the LAN backbone, and a database server running Oracle 10.2.0.1 Enterprise Edition.

Sphingolipid analysis

To confirmed the alteration of sphingomyelipids in SIRT1 KO mESCs, WT and SIRT1 KO mESCs cultured in serum-free ESGRO medium or serum-containing M10 medium were incubated with 5 μM BODIPY™ FL C5-Sphingomyelin (N-(4,4-Difluoro-5,7-Dimethyl-4-Bora-3a,4a-Diaza-s-Indacene-3-Pentanoyl)Sphingosyl Phosphocholine) (Invitrogen, D3522) or 5 μM BODIPY™ FL C5-Ceramide (N-(4,4-Difluoro-5,7-Dimethyl-4-Bora-3a,4a-Diaza-s-Indacene-3-Pentanoyl)Sphingosine) (Invitrogen, D3521) together with 5 μM delipidated BSA (as a delivery carrier) in Hanks' buffered salt solution containing 10 mM HEPES (HBSS/HEPES buffer pH 7.4) at 4 ºC for 30 min to load SM/ceramide. They were then incubated in medium without BODIPY FL C_5-Sphingolipid at 37 ºC for additional 30 min. The intensity of cellular BODIPY FL C5-Sphingomyelin/Ceramide were analyzed by Zeiss LSM 780 UV confocal microscope and by Flow cytometry analysis (Abs 505 nm and Em 511 nm).

To analyze the degradation of sphingomyelins, WT and SIRT1 KO mESCs were pre-load with BODIPY™ FL C5-Sphingomyelin at 4 ºC for 30 min. They were then incubated in medium without BODIPY FL C_5-Sphingomyelin at 37 ºC, and the dynamics of loaded BODIPY FL C_5-Sphingomyelins in cells were followed using Zeiss LSM 780 UV confocal microscope for additional 12 hours at 37 °C.

546 The relative contents of endogenous sphingomyelins in WT and SIRT1 KO mESCs
547 were analyzed using a commercially available Sphingomyelin Assay Kit (Abcam
548 ab133118) per manufacturer's instruction.
549
550 **Quantitative real-time PCR (qPCR)**
551 Total RNAs were isolated from mESCs or mice tissues using Qiagen RNeasy mini-kit
552 (74104). The nuclear and cytoplasmic RNA were separated and enriched by Fisher
553 BioReagents™ SurePrep™ Nuclear or Cytoplasmic RNA Purification Kit (Fisher Scientific,
554 BP280550). The cDNA was synthesized with ABI High-Capacity cDNA Reverse
555 Transcription Kits (4374967) and further analyzed with qPCR using SYBR Green
556 Supermix (Applied Biosystems). Three biological replications are performed for each
557 experiment and raw data are normalized to the expression level of Rplp0 mRNA levels.
558 The primers used in RT-PCR are listed in (Table S4).
559
560 **Immunofluorescence analysis**
561 mESCs grown on 0.1% gelatin coated coverslips were washed with PBS and fixed with
562 4% paraformaldehyde (PFA) in PBS (pH 7.4) solution for 20 minutes at room temperature.
563 They were then incubated with 1% glycine/PBS for 10 minutes, and cell membrane was
564 permeabilized with 0.3% Triton X-100 in 1% glycine/PBS for 10 minutes. Cells were further
565 blocked with 1% BSA and 0.05% Tween 20 in PBS for 30 minutes, incubated with primary
566 antibodies (Table S5) diluted with the blocking solution for overnight at 4°C, then the
567 secondary antibodies Alexa Fluor 488, 594 and 633 (for flow cytometry sorting) (Invitrogen,
568 A-11008, A-11032, A-21052) at 1:1000 in PBS for 1 hour at room temperature. Cells were
569 counterstained for Nuclei with DRAQ5™ Fluorescent Probe Solution (Thermal Fisher,
570 62251) or directly mounted on glass slides with VECTASHIELD® Antifade Mounting

571 Media (VECTOR LABORATORY) which contains DAPI. The images of stained cells are
572 acquired by Zeiss LSM 780 UV confocal microscope.
573
574 **Northern blotting**
575 The probe for Northern Blot hybridization is generated by using North2South™ Biotin
576 Random Prime Labeling Kit (Thermo, 17075). A 100ng DNA product, which was
577 synthesized from PCR reaction by using primer pair "5'-
578 CACCGCTAGCGCCACCatgacgctgctcgggtggctgata-3' and 5'-
579 CACCGCGGCCGCtaacacctccagtacgtgcaggct-3'" and the cDNA synthesized from total
580 RNA isolated from mESCs, was used as a template to yield biotin-labelled single strand
581 DNA probe that covers the full length Smpdl3b mRNA sequence. 40 µg of total RNA
582 isolated from mESC were separated with agarose electrophoresis with RNA Gel Loading
583 Dye (2X) (Thermo, R0641) and NorthernMax™ 10X Running Buffer (Ambion, AM8671).
584 The separated total RNA samples were further transblotted to positively charged nylon
585 transfer membrane (Cat. 77016) by using S & S TurboBlotter Rapid Downward Transfer
586 System (DAIGGER, EF77803) and SSC buffer (Thermo, AM9763). The RNA samples
587 transferred to membrane were further crosslinked by using Stratalinker® UV Crosslinker
588 (Model 1800) immediately upon completion of transblotting. The hybridization was
589 performed by using North2South® Chemiluminescent Hybridization and Detection Kit
590 (Thermo,17097) and the signaling of positive hybridization on membrane was detected
591 with Chemiluminescent Nucleic Acid Detection Module (Thermo, 89880). All procedures
592 were performed by strictly following protocols for each kit provided by manufacturers.
593
594 **Immunoblotting**
595 Cells were washed once with PBS, and were then lysed and scraped with 1 x SDS loading
596 buffer without bromophenol blue. Samples were boiled for 10 minutes, and quantified.

Equal amount of protein lysates was loaded and resolved on SDS-PAGE gel and transferred onto an PVDF membrane (Millipore). Blots were blocked with 5% BSA for 1 hour, incubated with primary antibodies at 4^{o}C overnight, incubated with secondary antibodies for 2 hours, and detected by Odyssey (LI-Cor inc.).

Chromatin Immunoprecipitation (ChIP)

To determine the association of RNA polymerase II (Pol II), c-Myc, EZH2, and histone marks H3K9me2, H3K4me3 and H3K27me3 on mouse Smpdl3b locus in WT and SIRT1 KO mESCs, cells were fixed, harvested, and sonicated. The resulting sonicated chromatin was processed for immunoprecipitation with respective antibodies (Table S5) as previously described (56) .

RNA-seq analysis

Total RNA was extracted from WT and SIRT1 KO mESCs cultured in ESGRO medium in triplicates. All RNA-seq libraries were prepared with the TruSeq Stranded/Ribo kit (Illumina, San Diego, CA) and sequenced using the pair-end 76bp protocol at about 520 million reads per library using the NovaSeq platform (Illumina) per the manufacturer's protocol. Adaptor sequences were removed by Trim Galore (v0.4.4). Then reads were aligned to mouse genome version GRCm38/mm10 using STAR (v2.5.3a) with Gencode vM18 annotation. Gene expression values were quantified using RSEM (v1.2.28) and differences in gene expression between experimental conditions were estimated using R package DEseq2 (Fold change > 2 were used as cutoff for downregulated genes).

Gene set enrichment analysis (GSEA) (v4.1.0) was implemented against all gene ontology (GO) gene sets in Molecular Signatures database (MsigDB v7.2) with 10000 permutations (min size 15, max size 500, FDR q < 0.25).

Promoter analysis of *Smpdl3b* gene

Potential transcription factors (TFs) on the promoter of Smpdl3b gene were predicted using "Match" from geneXplain (genexplain.com), in which the association scores, including "Core Motif Similarity" and "Weight Matrix Similarity" were calculated (54). A higher score implies a higher chance of the gene being the target of this TF.

Inhibition of c-Myc or EZH2 in mESCs

To test the possible roles of transcriptional factor c-Myc and EZH2 in regulation of *Smpdl3b* expression in mESCs, WT and SIRT1 KO mESCS were treated with c-Myc Inhibitor CAS 403811-55-2–Calbiochem (10058-F4) (Millipore Sigma, 475956) at 10 μM or EZh2 inhibitor Tazemetostat (EPZ-6438) (MCE, HY-13803) at indicated concentrations for 48 hours. WT and SIRT1 KO mESCs were also transfected with siRNA against mouse c-Myc (Santa Cruz, sc-29227) or EZH2 (ThermoFisher, 4390771) to knockdown their expression respectively. Cells were collected for 48 hours after transfection for qPCR analysis.

Site-direct mutagenesis

To further determine the influence of the acetylation status of c-Myc on expression of *Smpdl3b*, mouse c-Myc protein was first cloned into the pPHAGE-EF1α-HA-Puro vector. The major acetylation site of c-Myc protein, K323, was then mutated to either R to mimic deacetylated c-Myc (K323R) or Q to mimic acetylated c-Myc (K323Q) using QuickChange II Site-Directed Mutagenesis Kit (Agilent Technologies, 200522-5) against pPHAGE-EF1α-HA-Puro-c-Myc. pPHAGE-EF1α-HA-Puro vector, WT, K323R, and K323Q c-Myc constructs were transfected into WT and SIRT1 KO mESCs using Lipofectamine 3000 Reagent (Invitrogen, L3000001). The overexpression of WT and mutant c-Myc protein in

cells were confirmed by immunofluorescence staining of transfected cells with anti-c-Myc antibody (Abcam). The sequences of cloning primers were listed in Table S4.

Luciferase assay

To directly analyze the transcriptional regulation of *Smpdl3b* expression by c-Myc/SIRT1, firefly luciferase reporters driven by a 3.1 kb mouse *Smpdl3b* promoter fragment (amplified by 5'- tcttacgcgtgctagcccgggctcgagACTCATCCAAAGGACCCAGGTT-3' and 5'-tttatgtttttggcgtcttCCATGGGGCAGCAGGCACACATG-3') containing either wild type (WT) or a mutant c-Myc binding site (E-box) were cloned into pGL3 basic vector. The E-box mutant was constructed with QuikChange II XL Site-Directed Mutagenesis Kit (Agilent Technologies) using primers 5'-cgcgggttcccaccttgtggccagaagatcttctgggcagaactactcgtttggc-3' and 5'-gccaaacgagtagttctgcccagaagatcttctggccacaaggtgggaacccgcg-3'. The WT or mutant plasmids were then transfected into WT and SIRT1 KO mESCs together with the control pRL-TK plasmid (Renilla Luciferase, Promega). Cells were cultured for 48 h and the luciferase activity was measured using the Dual-Luciferase Reporter Assay System (Promega). The final firefly luciferase activity was normalized to the co-expressed renilla luciferase activity.

Measurement of membrane fluidity

WT and SIRT1 KO mESCs were seeded on glass cover slips and cultured in ESGRO medium overnight. They were then preincubated for 1 hour with or without 2.5 mM MβCD, and stained with 5 μM di-4-ANEPPDHQ for 30 minutes. Coverslips were mounted using ProLong®Gold (Invitrogen), images were acquired on a Zeiss LSM780 confocal microscope. The fluorescent dye was excited at 488 nm and images from 30 individual colonies in each group were acquired at 560 nm for emission from ordered phase and 620

nm for emission from disordered phase. The images were further analyzed ImageJ according to a method described previously (57).

In vitro neural differentiation of mESCs

In vitro neural differentiation of WT and SIRT1 KO mESCs were performed essentially as described (38, 39). Specifically, WT and SIRT1 KO mESCs maintained in ESGRO Complete PLUS Clonal Grade Medium (Millipore SF001-500P) were gently dissociated with 0.05% Trypsin and plated onto 0.1% gelatin coated cell culture dish at a density of $1x10^4$cells / cm^2 with RHB-A medium (Clontech TaKaba Cellartis, Y40001). Medium was changed every 2 days and cultured for 4 days. Cells were then dissociated with 0.05% Trypsin again and plated into cell culture dish coated with 1 µg/ml Laminin (Sigma, L2020) at a density of $2x10^4$cells/cm^2 in RHB-A medium supplemented with 5 ng/ml murine bFGF (Sigma, SRP4038-50UG). Medium was changed again every 2 days for the next 3 weeks. Cell morphology was monitored during the differentiation. The differentiated neural cells were maintained in RHB-A: Neurobasal (ThermoFisher,10888022): B27 Supplement (ThermoFisher,17504044) (1:1:0.02) medium to for a better survival.

FACS analysis

To quantify the factions of differentiated cells at different stages during *in vitro* neural differentiation, differentiated cells were harvested with trypsin and fixed with 4% PFA. After fixation, cells are washed with PBS and immunofluorescence stained with different neural markers, and analyzed by FACS.

Alkaline phosphatase staining

The alkaline phosphatase staining assay was performed using the Alkaline Phosphatase staining kit II as per manufacturer's instructions (Stemgent, Cambridge, MA; cat. no. 00-0055).

Maternal high-fat diet feeding

To investigate the effects of maternal high-fat diet feeding on embryonic development of control and SIRT1 KO mice, 6-8 weeks old SIRT1 heterozygous (*Sirt1*$^{+/-}$) female mice were fed with either control chow diet (NIH-31 contains 4% fat) or a high-fat diet (D12492 contains 36% fat) for 4-8 weeks. They were then bred with age matched *Sirt1*$^{+/-}$ male mice fed with chow diet. Early next morning, females with the mating plug (E0.5) were separated from the males into a new cage and put back on the high-fat diet. Embryos from E14.5 and E18.5 were then collected and analyzed. The total feeding time on the high-fat diet is up to 11 weeks. Embryos were collected from at least 4 dams (pregnant females) for each time point, this sample size was estimated using Chi square based on 100% penetrance of body weight reduction of SIRT1 KO embryos and a 95% power.

All animal procedures were reviewed and approved by National Institute of Environmental Health Sciences Animal Care and Use Committee. All animals were housed, cared for, and used in compliance with the *Guide for the Care and Use of Laboratory Animals* and housed and used in an Association for the Assessment and Accreditation of Laboratory Animal Care, International (AAALAC) Program.

Quantification and statistical analysis

Values are expressed as mean ± standard error of mean (SEM) from at least three independent experiments or biological replicates, unless otherwise indicated in the figure legend. Significant differences between the means were analyzed by the two-tailed, unpaired, Student's t-test, and differences were considered significant at *$p<0.05$ using

Microsoft Office Excel (Version 16.16.27). No methods were used to determine whether the data met assumptions of the statistical approach (e.g. test for normal distribution).

Bioinformatic analyses of RNA-seq data are detailed in METHOD DETAILS section.

Data availability

The RNA-seq (RNA-seq) data have been deposited to Gene Expression Omnibus under the accession number GSE163920 (https://www.ncbi.nlm.nih.gov/geo/query/acc.cgi?acc=GSE163920). The secure token for reviewers is cryvqkekdbufrmb.

Additional information on DEGs is available from Table S3.

Metabolomics data (lipid alterations) between WT and SIRT1 KO mESCs is available in Table S1.

Sphingolipid profiles between WT and SIRT1 KO mESCs and hESCs are available in Table S2.

All oligos used in the study are available in Table S4.

All antibodies used in the study are available in Table S5.

List of Supplemental Tables

Table S1. Lipid alterations in WT and SIRT1 KO mESCs analyzed by metabolomics.

Table S2. Accumulation of sphingomyelin in both SIRT1 KO hESCs and mESCs.

Table S3. Significantly differentially expressed genes between SIRT1 KO vs WT mESCs.

Table S4. Oligonucleotides used in the study.

Table S5. Antibodies used in the study.

Acknowledgements

We thank Drs. Serena Dudek, Anton Jetten, and members of the Li laboratory for critical reading of the manuscript. We also thank NIEHS Epigenomics Core Facility for performing RNA-seq experiments. This research was supported by the Intramural Research Program of National Institute of Environmental Health Sciences of the NIH Z01 ES102205 (to X. L.). This study was also supported in part by grants from National Nature Science Foundation of China (NSFC) 31730110 and 31661143031 (to Z. W.) and NIH grants R01CA230631 and R01DK111430 (to J. X.). J. X. is a Scholar of The Leukemia & Lymphoma Society (LLS). X. F. is supported by a fellowship from China Postdoctoral Science Foundation (2020M681437).

Author contributions

W. F. designed and performed experiments, analyzed data, and wrote the manuscript. S. T. designed and performed experiments and analyzed data. X. F. analyzed RNA-seq data. Y. F. generated SIRT1 KO hESCs and analyzed the metabolic profiles. X. X., J. L., and L. L. analyzed mouse *Smpdl3b* promoter. J. X. provided dCas9 mESCs. Z. W. guided and coordinated the study and analyzed data. X. L. guided, designed, and coordinated the study, analyzed data, and wrote the manuscript. All authors critically reviewed the manuscript.

Conflict of interest statement

The authors declare no conflict of interest.

References

1. Chen Y, Liu Y, Sullards MC, Merrill AH, Jr. An introduction to sphingolipid metabolism and analysis by new technologies. Neuromolecular Med. 2010;12(4):306-19.
2. Merrill AH, Jr., Wang MD, Park M, Sullards MC. (Glyco)sphingolipidology: an amazing challenge and opportunity for systems biology. Trends Biochem Sci. 2007;32(10):457-68.
3. Pralhada Rao R, Vaidyanathan N, Rengasamy M, Mammen Oommen A, Somaiya N, Jagannath MR. Sphingolipid metabolic pathway: an overview of major roles played in human diseases. J Lipids. 2013;2013:178910.
4. Hannun YA, Obeid LM. Principles of bioactive lipid signalling: lessons from sphingolipids. Nat Rev Mol Cell Biol. 2008;9(2):139-50.
5. van Meer G, Voelker DR, Feigenson GW. Membrane lipids: where they are and how they behave. Nat Rev Mol Cell Biol. 2008;9(2):112-24.
6. Brown DA, London E. Structure and origin of ordered lipid domains in biological membranes. J Membr Biol. 1998;164(2):103-14.
7. Heinz LX, Baumann CL, Koberlin MS, Snijder B, Gawish R, Shui G, et al. The Lipid-Modifying Enzyme SMPDL3B Negatively Regulates Innate Immunity. Cell Rep. 2015;11(12):1919-28.
8. Mitrofanova A, Mallela SK, Ducasa GM, Yoo TH, Rosenfeld-Gur E, Zelnik ID, et al. SMPDL3b modulates insulin receptor signaling in diabetic kidney disease. Nat Commun. 2019;10(1):2692.
9. Choi S, Snider AJ. Sphingolipids in High Fat Diet and Obesity-Related Diseases. Mediators Inflamm. 2015;2015:520618.
10. Giusto NM, Roque ME, Ilincheta de Boschero MG. Effects of aging on the content, composition and synthesis of sphingomyelin in the central nervous system. Lipids. 1992;27(11):835-9.
11. Lightle SA, Oakley JI, Nikolova-Karakashian MN. Activation of sphingolipid turnover and chronic generation of ceramide and sphingosine in liver during aging. Mech Ageing Dev. 2000;120(1-3):111-25.
12. Tacconi MT, Lligona L, Salmona M, Pitsikas N, Algeri S. Aging and food restriction: effect on lipids of cerebral cortex. Neurobiol Aging. 1991;12(1):55-9.
13. Muthusamy T, Cordes T, Handzlik MK, You L, Lim EW, Gengatharan J, et al. Serine restriction alters sphingolipid diversity to constrain tumour growth. Nature. 2020;586(7831):790-5.
14. Brice SE, Cowart LA. Sphingolipid metabolism and analysis in metabolic disease. Adv Exp Med Biol. 2011;721:1-17.
15. Alvarez-Vasquez F, Sims KJ, Cowart LA, Okamoto Y, Voit EO, Hannun YA. Simulation and validation of modelled sphingolipid metabolism in Saccharomyces cerevisiae. Nature. 2005;433(7024):425-30.
16. Houtkooper RH, Pirinen E, Auwerx J. Sirtuins as regulators of metabolism and healthspan. Nat Rev Mol Cell Biol. 2012;13(4):225-38.
17. Tang S, Huang G, Fan W, Chen Y, Ward JM, Xu X, et al. SIRT1-Mediated Deacetylation of CRABPII Regulates Cellular Retinoic Acid Signaling and Modulates Embryonic Stem Cell Differentiation. Mol Cell. 2014;55(6):843-55.
18. Han MK, Song EK, Guo Y, Ou X, Mantel C, Broxmeyer HE. SIRT1 regulates apoptosis and Nanog expression in mouse embryonic stem cells by controlling p53 subcellular localization. Cell Stem Cell. 2008;2(3):241-51.
19. McBurney MW, Yang X, Jardine K, Hixon M, Boekelheide K, Webb JR, et al. The mammalian SIR2alpha protein has a role in embryogenesis and gametogenesis. Mol Cell Biol. 2003;23(1):38-54.

20. Cheng HL, Mostoslavsky R, Saito S, Manis JP, Gu Y, Patel P, et al. Developmental defects and p53 hyperacetylation in Sir2 homolog (SIRT1)-deficient mice. Proc Natl Acad Sci U S A. 2003.
21. Wang RH, Sengupta K, Li C, Kim HS, Cao L, Xiao C, et al. Impaired DNA damage response, genome instability, and tumorigenesis in SIRT1 mutant mice. Cancer Cell. 2008;14(4):312-23.
22. Dietrich MO, Antunes C, Geliang G, Liu ZW, Borok E, Nie Y, et al. Agrp neurons mediate Sirt1's action on the melanocortin system and energy balance: roles for Sirt1 in neuronal firing and synaptic plasticity. J Neurosci. 2010;30(35):11815-25.
23. Ramadori G, Fujikawa T, Fukuda M, Anderson J, Morgan DA, Mostoslavsky R, et al. SIRT1 deacetylase in POMC neurons is required for homeostatic defenses against diet-induced obesity. Cell Metab. 2010;12(1):78-87.
24. Ramadori G, Fujikawa T, Anderson J, Berglund ED, Frazao R, Michan S, et al. SIRT1 deacetylase in SF1 neurons protects against metabolic imbalance. Cell Metab. 2011;14(3):301-12.
25. Satoh A, Brace CS, Rensing N, Cliften P, Wozniak DF, Herzog ED, et al. Sirt1 extends life span and delays aging in mice through the regulation of Nk2 homeobox 1 in the DMH and LH. Cell Metab. 2013;18(3):416-30.
26. Hisahara S, Chiba S, Matsumoto H, Tanno M, Yagi H, Shimohama S, et al. Histone deacetylase SIRT1 modulates neuronal differentiation by its nuclear translocation. Proc Natl Acad Sci U S A. 2008;105(40):15599-604.
27. Michan S, Li Y, Chou MM, Parrella E, Ge H, Long JM, et al. SIRT1 is essential for normal cognitive function and synaptic plasticity. J Neurosci. 2010;30(29):9695-707.
28. Gao J, Wang WY, Mao YW, Graff J, Guan JS, Pan L, et al. A novel pathway regulates memory and plasticity via SIRT1 and miR-134. Nature. 2010;466(7310):1105-9.
29. Herskovits AZ, Guarente L. SIRT1 in neurodevelopment and brain senescence. Neuron. 2014;81(3):471-83.
30. Tang S, Fang Y, Huang G, Xu X, Padilla-Banks E, Fan W, et al. Methionine metabolism is essential for SIRT1-regulated mouse embryonic stem cell maintenance and embryonic development. EMBO J. 2017;36(21):3175-93.
31. Wakayama T, Rodriguez I, Perry AC, Yanagimachi R, Mombaerts P. Mice cloned from embryonic stem cells. Proc Natl Acad Sci U S A. 1999;96(26):14984-9.
32. Menssen A, Hydbring P, Kapelle K, Vervoorts J, Diebold J, Luscher B, et al. The c-MYC oncoprotein, the NAMPT enzyme, the SIRT1-inhibitor DBC1, and the SIRT1 deacetylase form a positive feedback loop. Proc Natl Acad Sci U S A. 2012;109(4):E187-96.
33. Liu X, Zhang Y, Chen Y, Li M, Zhou F, Li K, et al. In Situ Capture of Chromatin Interactions by Biotinylated dCas9. Cell. 2017;170(5):1028-43 e19.
34. Yin X, Giap C, Lazo JS, Prochownik EV. Low molecular weight inhibitors of Myc-Max interaction and function. Oncogene. 2003;22(40):6151-9.
35. Wan J, Zhan J, Li S, Ma J, Xu W, Liu C, et al. PCAF-primed EZH2 acetylation regulates its stability and promotes lung adenocarcinoma progression. Nucleic Acids Res. 2015;43(7):3591-604.
36. Bieberich E. Ceramide signaling in cancer and stem cells. Future Lipidol. 2008;3(3):273-300.
37. Wang G, Spassieva SD, Bieberich E. Ceramide and S1P Signaling in Embryonic Stem Cell Differentiation. Methods Mol Biol. 2018;1697:153-71.
38. Ying QL, Nichols J, Chambers I, Smith A. BMP induction of Id proteins suppresses differentiation and sustains embryonic stem cell self-renewal in collaboration with STAT3. Cell. 2003;115(3):281-92.

871 39. Abranches E, Silva M, Pradier L, Schulz H, Hummel O, Henrique D, et al. Neural
872 differentiation of embryonic stem cells in vitro: a road map to neurogenesis in the embryo.
873 PLoS One. 2009;4(7):e6286.
874 40. van Echten-Deckert G, Herget T. Sphingolipid metabolism in neural cells. Biochim
875 Biophys Acta. 2006;1758(12):1978-94.
876 41. Olsen ASB, Faergeman NJ. Sphingolipids: membrane microdomains in brain
877 development, function and neurological diseases. Open Biol. 2017;7(5).
878 42. Piccinini M, Scandroglio F, Prioni S, Buccinna B, Loberto N, Aureli M, et al.
879 Deregulated sphingolipid metabolism and membrane organization in neurodegenerative
880 disorders. Mol Neurobiol. 2010;41(2-3):314-40.
881 43. Canto C, Auwerx J. Caloric restriction, SIRT1 and longevity. Trends Endocrinol
882 Metab. 2009;20(7):325-31.
883 44. Imai S. SIRT1 and caloric restriction: an insight into possible trade-offs between
884 robustness and frailty. Curr Opin Clin Nutr Metab Care. 2009;12(4):350-6.
885 45. Prozorovski T, Schulze-Topphoff U, Glumm R, Baumgart J, Schroter F,
886 Ninnemann O, et al. Sirt1 contributes critically to the redox-dependent fate of neural
887 progenitors. Nat Cell Biol. 2008;10(4):385-94.
888 46. Kang MR, Lee SW, Um E, Kang HT, Hwang ES, Kim EJ, et al. Reciprocal roles of
889 SIRT1 and SKIP in the regulation of RAR activity: implication in the retinoic acid-induced
890 neuronal differentiation of P19 cells. Nucleic Acids Res. 2009;38(3):822-31.
891 47. Fusco S, Leone L, Barbati SA, Samengo D, Piacentini R, Maulucci G, et al. A
892 CREB-Sirt1-Hes1 Circuitry Mediates Neural Stem Cell Response to Glucose Availability.
893 Cell Rep. 2016;14(5):1195-205.
894 48. Bernstein BE, Mikkelsen TS, Xie X, Kamal M, Huebert DJ, Cuff J, et al. A bivalent
895 chromatin structure marks key developmental genes in embryonic stem cells. Cell.
896 2006;125(2):315-26.
897 49. Sanz LA, Chamberlain S, Sabourin JC, Henckel A, Magnuson T, Hugnot JP, et al.
898 A mono-allelic bivalent chromatin domain controls tissue-specific imprinting at Grb10.
899 EMBO J. 2008;27(19):2523-32.
900 50. Vastenhouw NL, Schier AF. Bivalent histone modifications in early embryogenesis.
901 Curr Opin Cell Biol. 2012;24(3):374-86.
902 51. Iessa N, Berard A. Update on Prepregnancy Maternal Obesity: Birth Defects and
903 Childhood Outcomes. J Pediatr Genet. 2015;4(2):71-83.
904 52. Helle E, Priest JR. Maternal Obesity and Diabetes Mellitus as Risk Factors for
905 Congenital Heart Disease in the Offspring. J Am Heart Assoc. 2020;9(8):e011541.
906 53. Tong L, Kalish BT. The impact of maternal obesity on childhood neurodevelopment.
907 J Perinatol. 2020.
908 54. Chen X, Xu H, Yuan P, Fang F, Huss M, Vega VB, et al. Integration of external
909 signaling pathways with the core transcriptional network in embryonic stem cells. Cell.
910 2008;133(6):1106-17.
911 55. Evans AM, Bridgewater BR, Miller LAD, Mitchell MW, Robinson RJ, Dai H, et al.
912 High Resolution Mass Spectrometry Improves Data Quantity and Quality as Compared to
913 Unit Mass Resolution Mass Spectrometry in High-Throughput Profiling Metabolomics.
914 Metabolomics. 2014;4(2).
915 56. Shimbo T, Du Y, Grimm SA, Dhasarathy A, Mav D, Shah RR, et al. MBD3 localizes
916 at promoters, gene bodies and enhancers of active genes. PLoS Genet.
917 2013;9(12):e1004028.
918 57. Owen DM, Williamson D, Magenau A, Gaus K. Optical techniques for imaging
919 membrane domains in live cells (live-cell palm of protein clustering). Methods Enzymol.
920 2012;504:221-35.
921

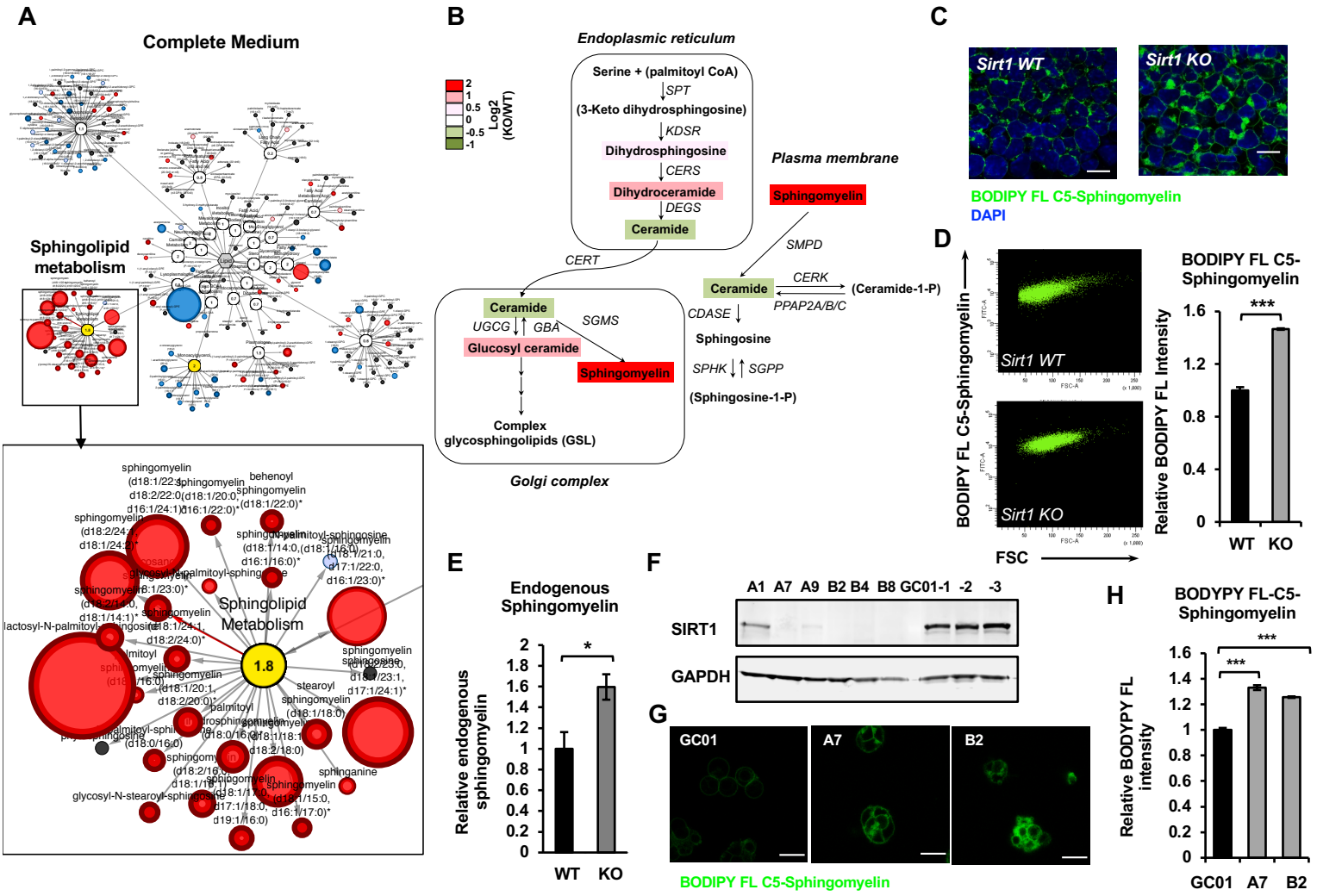

Figure 1. Deletion of SIRT1 in mESCs results in a dramatic accumulation of sphingomyelin.

(A) Metabolomic analysis reveals a massive accumulation of sphingolipids in SIRT1 KO mESCs. WT and SIRT1 KO mESCs were cultured in a complete mESC maintenance medium (M10) and metabolites were analyzed by metabolomics as described in Methods. The networks of significantly changed metabolites in lipid metabolism were analyzed by Cytoscape 2.8.3. Metabolites increased in SIRT1 KO mESCs were labeled red ($p<0.05$) or pink ($0.05<p<0.10$), metabolites decreased in SIRT1 KO mESCs were labeled blue ($p<0.05$) or light blue ($0.05<p<0.10$). Metabolite node size is proportional to the fold change in KO vs WT (n=5 biological replicates). (B) The relative abundance of different metabolites mapped into sphingolipid metabolism pathways. Metabolites in sphingolipid metabolism in WT and SIRT1 KO mESCs were analyzed as in (A) and the relative abundance of metabolites involved in sphingolipid metabolism was displayed by the heat map (n=5 biological replicates). (C-D) SIRT1 KO mESCs have increased levels of BODIPY FL-labeled sphingomyelin. WT and SIRT1 KO mESCs cultured in ESGRO medium were labeled with BODIPY FL-labeled sphingomyelin for 30 min at 4 □C then chased at 37 □C for 30 min. The intensity of BODIPY FL-labeled sphingomyelin in cells were analyzed by (C) confocal fluorescence imaging and by (D) quantitative FACS (n=3 biological replicates, ***$p<0.001$). Scale bars: 20μm. (E) SIRT1 KO mESCs have increased levels of endogenous sphingomyelin. WT and SIRT1 KO mESCs cultured in ESGRO medium were extracted and total levels of endogenous sphingomyelin were determined in extracts by an enzyme-coupled colorimetric assay as described in Methods (n=3 biological replicates, *$p<0.05$). (F-H) Deletion of SIRT1 in E14 mESCs leads to accumulation of sphingomyelin. (F) SIRT1 was deleted in E14 mESC line using crispr/cas9 mediated gene editing technology and (G) relative levels of BODIPY FL-labeled sphingomyelins were imaged and (H) measured (n=2 independent clones with 3 biological replicates for each clone, ***$p<0.001$). Scale bars: 20μm.

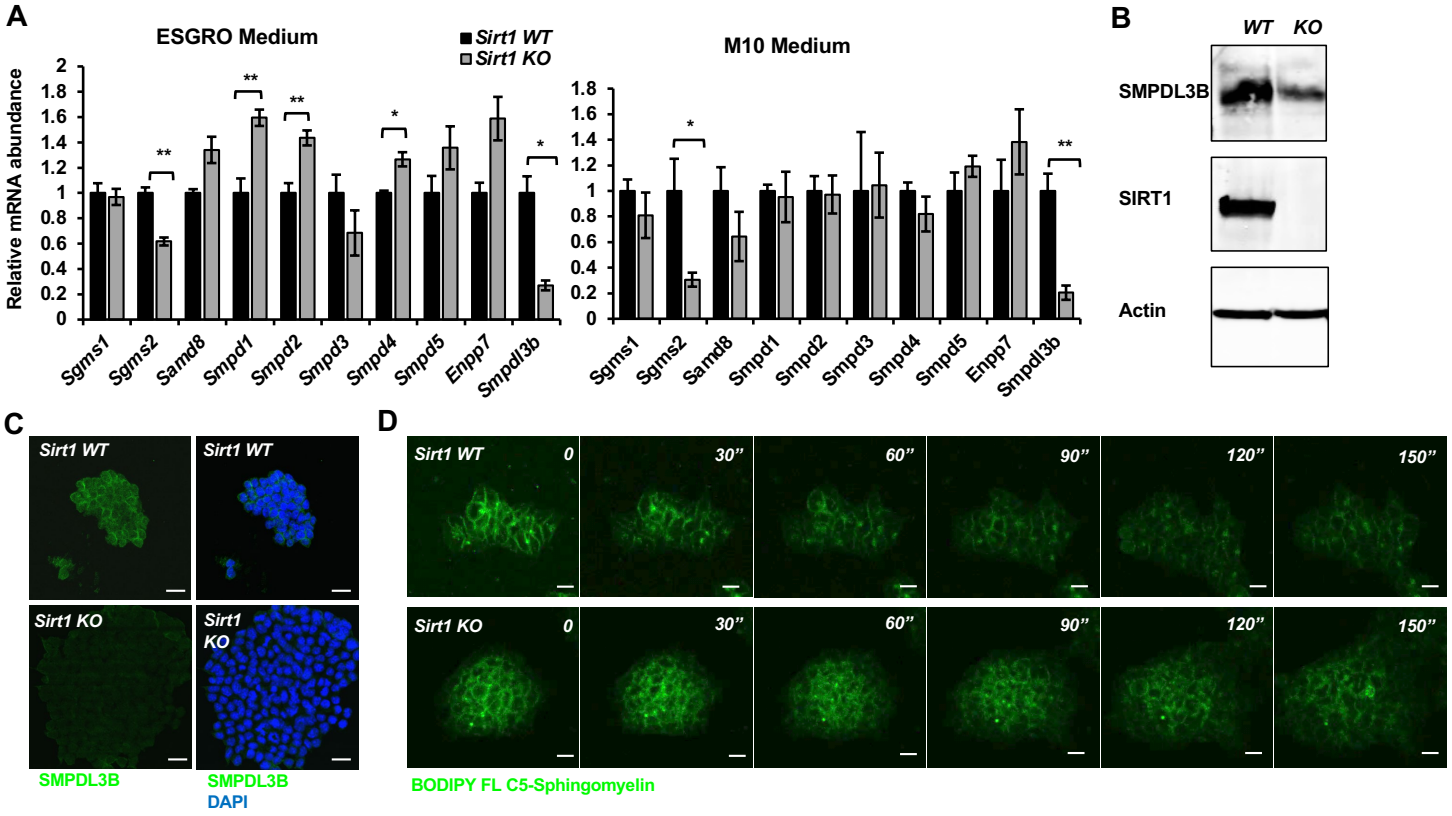

Figure 2. SIRT1 deficient mESCs have reduced expression of SMPDL3B and sphingomyelin degradation.

(A) SIRT1 KO mESCs have reduced mRNA levels of Smpdl3b. WT and SIRT1 KO mESCs were cultured in either ESGRO medium or M10 medium. The mRNA levels of indicated enzymes involved in sphingomyelin synthesis (Sgms) and degradation (Smpd) were analyzed by qPCR (n=3 biological replicates, *p<0.05, **p<0.01). (B-C) SIRT1 KO mESCs have reduced protein levels of SMPDL3B. The protein levels of SMPDL3B were analyzed by (B) immuno-blotting and (C) immuno-fluorescence staining. Scale bars: 20μm. (D) SIRT1 KO mESCs have reduced degradation of sphingomyelin. WT and SIRT1 KO mESCs were preloaded with BODIPY FL-C5 sphingomyelin for 30 min at 4 □C, then incubated with BODIPY FL-C5 sphingomyelin-free medium at 37 □C. The dynamic of BODIPY FL-sphingomyelin was monitored for additional 12 hours at 37 □C. WT and SIRT1 KO mESC clones that have comparable preloaded levels of BODIPY FL-C5 sphingomyelin were shown. Scale bars: 20μm.

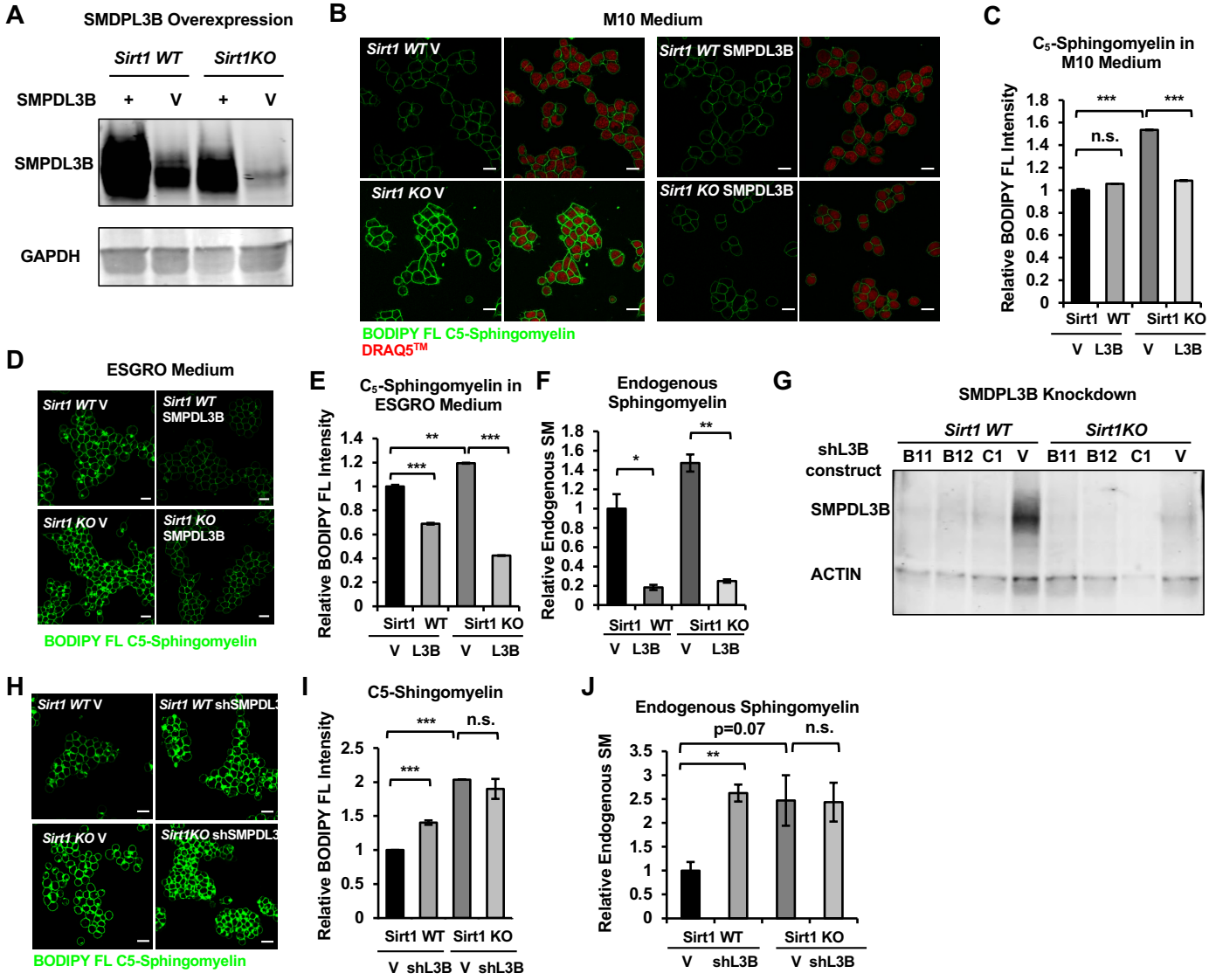

Figure 3. SMPDL3B directly controls the sphingomyelin contents in mESCs.

(A) Overexpression of SMPDL3B in mESCs. WT and SIRT1 KO mESCs were infected with lentiviral particles containing empty vector (V) or expressing SMPDL3B. The expression of SMPDL3B was analyzed by immuno-blotting. (B-C) Overexpression of SMPDL3B reduces sphingomyelin levels in mESCs cultured in M10 medium. The cellular levels of sphingomyelin in WT and SIRT1 KO mESCs with or without overexpression of SMPFL3B were analyzed by (B) BODIPY FL-sphingomyelin confocal imaging, and (C) FACS assay (n=3 biological replicates, *p<0.05, **p<0.01). Scale bars in (B): 20μm. L3B in (C): SMPDL3B. (D-F) Overexpression of SMPDL3B reduces sphingomyelin levels in mESCs cultured in ESGRO medium. The cellular levels of sphingomyelin in WT and SIRT1 KO mESCs with or without overexpression of SMPDL3B were analyzed by (D) BODIPY FL-sphingomyelin staining, (E) BODIPY FL-sphingomyelin FACS assay, or (F) an enzyme-coupled colorimetric assay for endogenous sphingomyelin. (n=3 biological replicates, *p<0.05, **p<0.01, ***p<0.001). Scale bars: 20μm. (G) Stable knockdown of the expression of SMPDL3B in mESCs. WT and SIRT1 KO mESCs were infected with lentiviral particles containing empty vector (V) or shRNA constructs for SMPDL3B (B11, B12, C1). The expression of SMPDL3B were analyzed by immuno-blotting. shL3B: shRNAs against SMPDL3B. (H-J) Knocking down SMPDL3B increases sphingomyelin levels in WT mESCs but not significantly further in SIRT1 KO mESCs in ESGRO medium. The cellular levels of sphingomyelin in WT and SIRT1 KO mESCs with or without stable knockdown of SMPDL3B were analyzed by (H) BODIPY FL-sphingomyelin confocal imaging, (I) BODIPY FL-sphingomyelin FACS assay, or (J) an enzyme-coupled colorimetric assay for endogenous sphingomyelin (n=3 biological replicates, **p<0.01, ***p<0.001). Scale bars: 20μm.

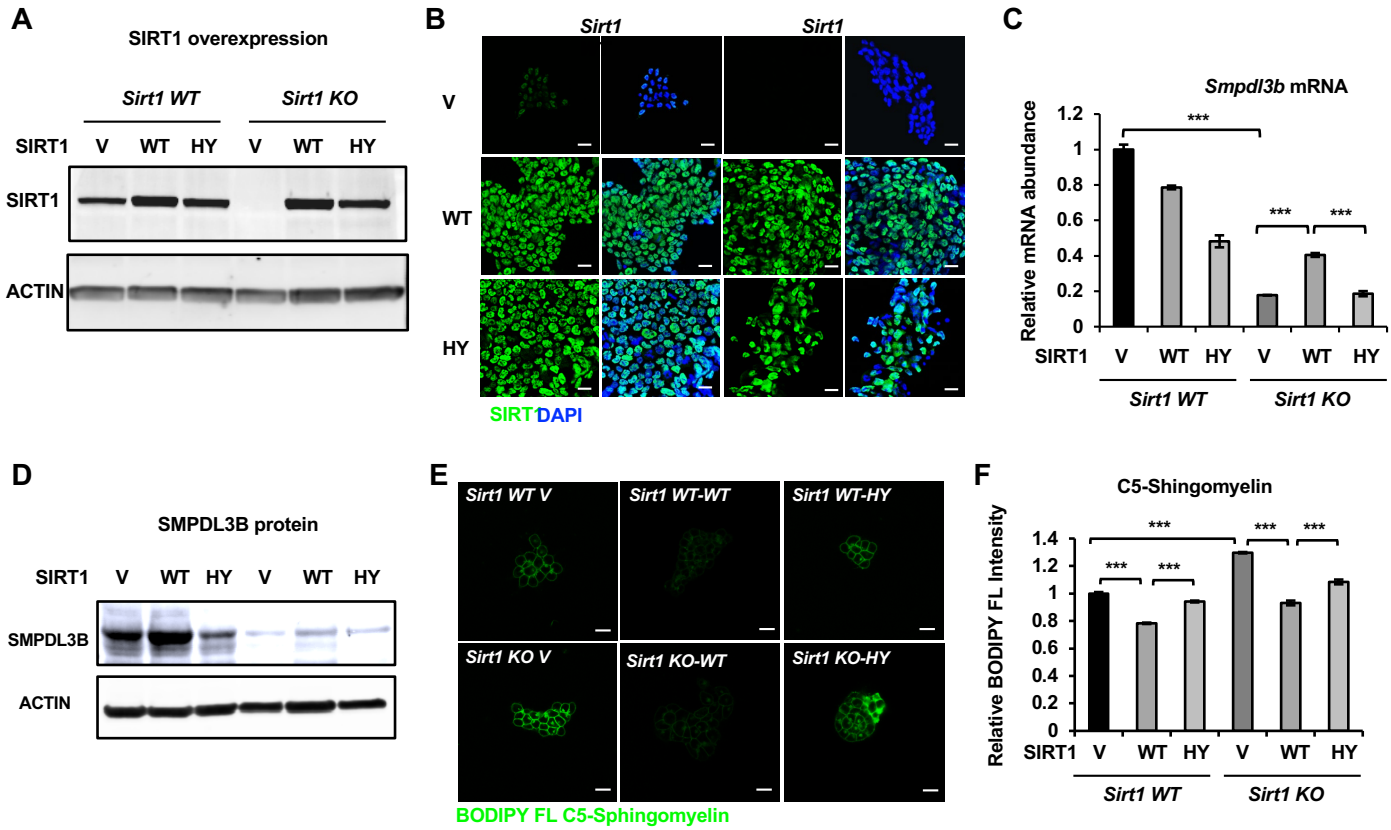

Figure 4. Expression of WT but not catalytically inactive SIRT1 partially rescues the sphingomyelin defect in SIRT1 KO mESCs.

(A-B) SIRT1 protein levels in indicated mESCs. WT and SIRT1 KO mESCs were infected with lentiviral particles containing empty vector (Plentill-EF1α) or constructs expressing WT or a catalytically inactive mutant SIRT1 (HY). The expression of SIRT1 was analyzed by either (A) immunoblotting or (B) immunofluorescence staining. Bars in B: 20μm. (C-D) Expression of the HY mutant SIRT1 represses the expression of Smpdl3b in WT mESCs, whereas expression of WT but not the HY mutant SIRT1 increases the expression of Smpdl3b in SIRT1 KO mESCs. The expression of SMPDL3B was analyzed by either (C) qPCR or (D) immunoblotting. (n=3 biological replicates, ***p<0.001). (E-F) Expression of WT but not HY mutant SIRT1 significantly reduces the sphingomyelin levels in both WT and SIRT1 KO mESCs. Indicated WT and SIRT1 KO mESCs cultured in ESGRO medium were labeled with BODIPY FL-labeled sphingomyelin for 30 min at 4 ℃ then incubated at 37 ℃ for 30 min. The intensity of BODIPY FL-labeled sphingomyelin in cells were analyzed by (E) confocal fluorescence imaging and by (F) quantitative FACS (n=3 biological replicates, ***p<0.001). Bars in E: 20μm.

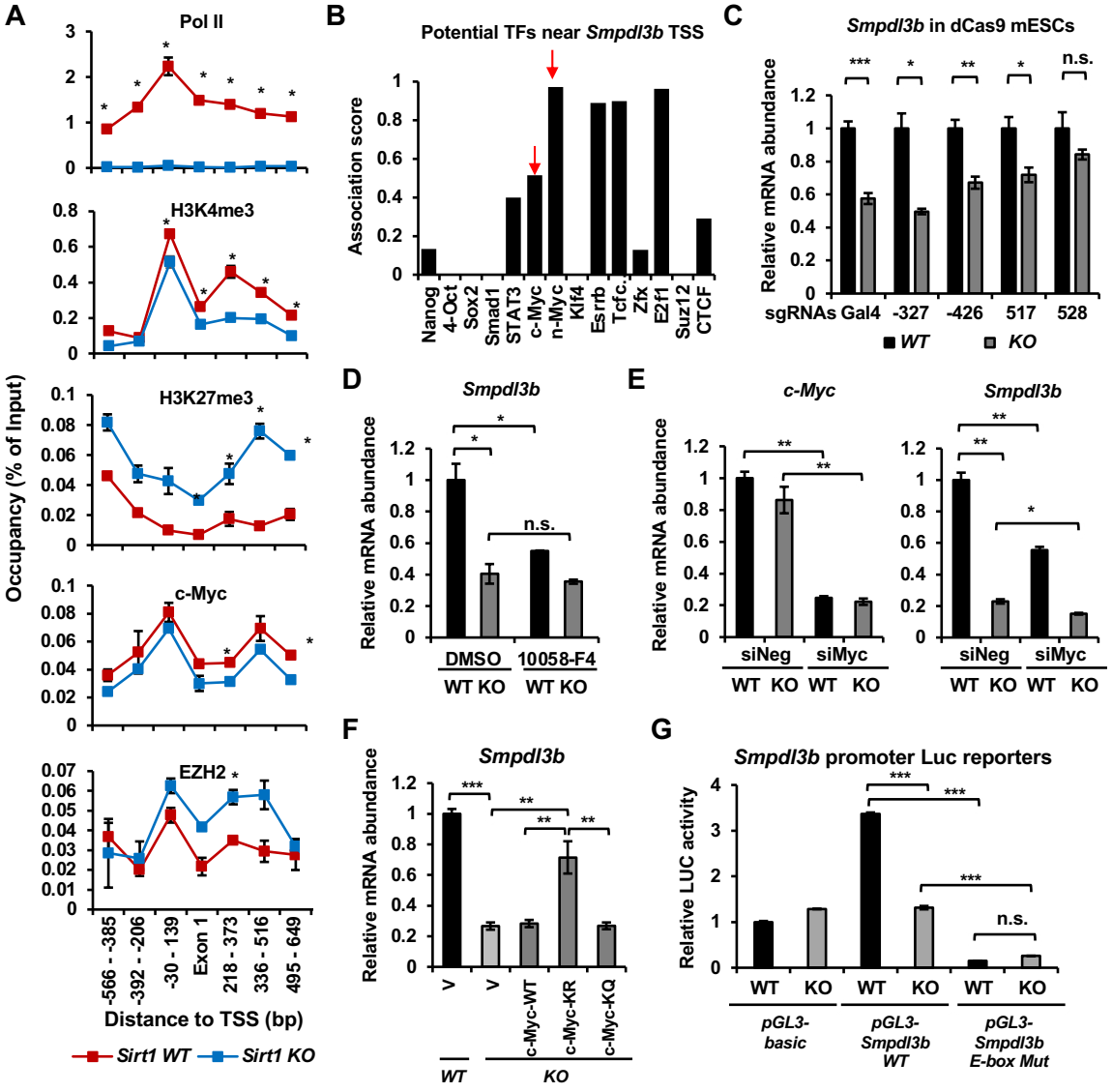

Figure 5. SIRT1 promotes the transcription of Smpdl3b through c-Myc in mESCs.

(A) SIRT1 KO mESCs have reduced transcription of Smpdl3b. WT and SIRT1 KO mESCs cultured in ESGRO medium were crosslinked and subjected for ChIP-qPCR profiling of PolII, c-Myc, EZH2, and indicated chromatin activation or repression marks near the TSS region of Smpdl3b gene (n=3 biological replicates, *p<0.05). (B) Association scores of potential transcription factors (TFs) near the TSS of Smpdl3b gene. The association scores of indicated TFs were obtained from a published dataset (54). A higher score is suggestive of a higher chance of Smpdl3b gene being targeted by the potential TF. (C) A guide RNA (gRNA) targeting the +528 locus at the TSS region of Smpdl3b gene rescues the expression of this gene. gRNAs targeting indicated loci near the TSS region of Smpdl3b gene were transfected into WT and SIRT1 KO mESCs stably expressing a dox-inducible dCas9 and BirA-V5 (dCas9 mESCs). The mRNA levels of Smpdl3b were analyzed by qPCR (n=3 biological replicates, *p<0.05, **p<0.01, ***p<0.001). (D) Inhibition of c-Myc activity reduces the expression of Smpdl3b gene in mESCs. WT and SIRT1 KO mESCs were treated with DMSO or 10 □M 10058-F4 for 48 hours. The mRNA levels of Smpdl3b were analyzed by qPCR (n=3 biological replicates, *p<0.05, **p<0.01, ***p<0.001). (E) Knocking down c-Myc significantly reduces the expression of Smpdl3b gene in mESCs. WT and SIRT1 KO mESCs were transfected with siRNAs against c-Myc for 48 hours. The mRNA levels of c-Myc and Smpdl3b were analyzed by qPCR (n=3 biological replicates, *p<0.05, **p<0.01). (F) Overexpression of the KR mutant of c-Myc partially reduces the expression of Smpdl3b gene in SIRT1 KO mESCs. The mRNA levels of Smpdl3b in indicated mESCs were analyzed by qPCR (n=6 biological replicates, **p<0.01, ***p<0.001). (G) Mutation of the c-Myc binding E-box element on the promoter of Smpdl3b gene abolishes the expression of Smpdl3b luciferase reporter in mESCs. Luciferase reporters containing the basic vector (pGL3-basic), the WT promoter of Smpdl3b gene, or a promoter of Smpdl3b gene with a mutant E-box were transfected into WT and SIRT1 KO mESCs, and the luciferase activities were measured as described in Methods (n=3 biological replicates, ***p<0.001).

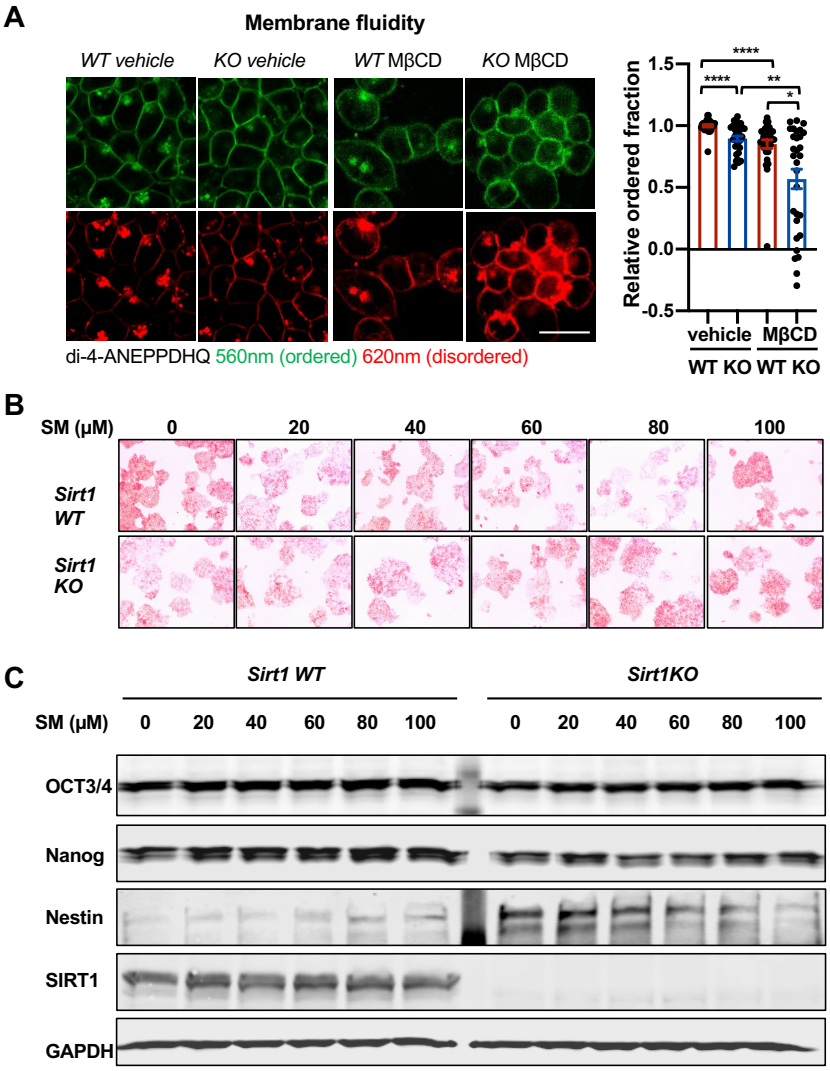

Figure 6. Sphingomyelin accumulation increases membrane fluidity and induces expression of Nestin in SIRT1 KO mESCs.

(A) SIRT1 KO mESCs have an increased membrane fluidity. WT and SIRT1 KO mESCs cultured in ESGRO medium were preincubated with or without 2.5 mM MβCD for 1 hour, then stained with 5 μM di-4-ANEPPDHQ for at least 30 minutes. The relative ordered fraction in each group was analyzed as described in Methods (n=30 clones/group, *p<0.05, **p<0.01, ***p<0.001, ****p<0.0001). Bars: 10μm. (B-C) Exogeneous sphingomyelin treatment increases Nestin but not pluripotency markers in mESCs. WT and SIRT1 KO mESCs were treated with indicated concentrations of sphingomyelin (SM) in ESGRO medium for 48 hours. (B) The intensity of AP was analyzed as described in Methods. (C) The protein abundance of pluripotency marker OCT3/4, Nanog and neuroepithelial stem cell marker Nestin in WT and Sirt1 KO mESCs were determined by immunoblotting.

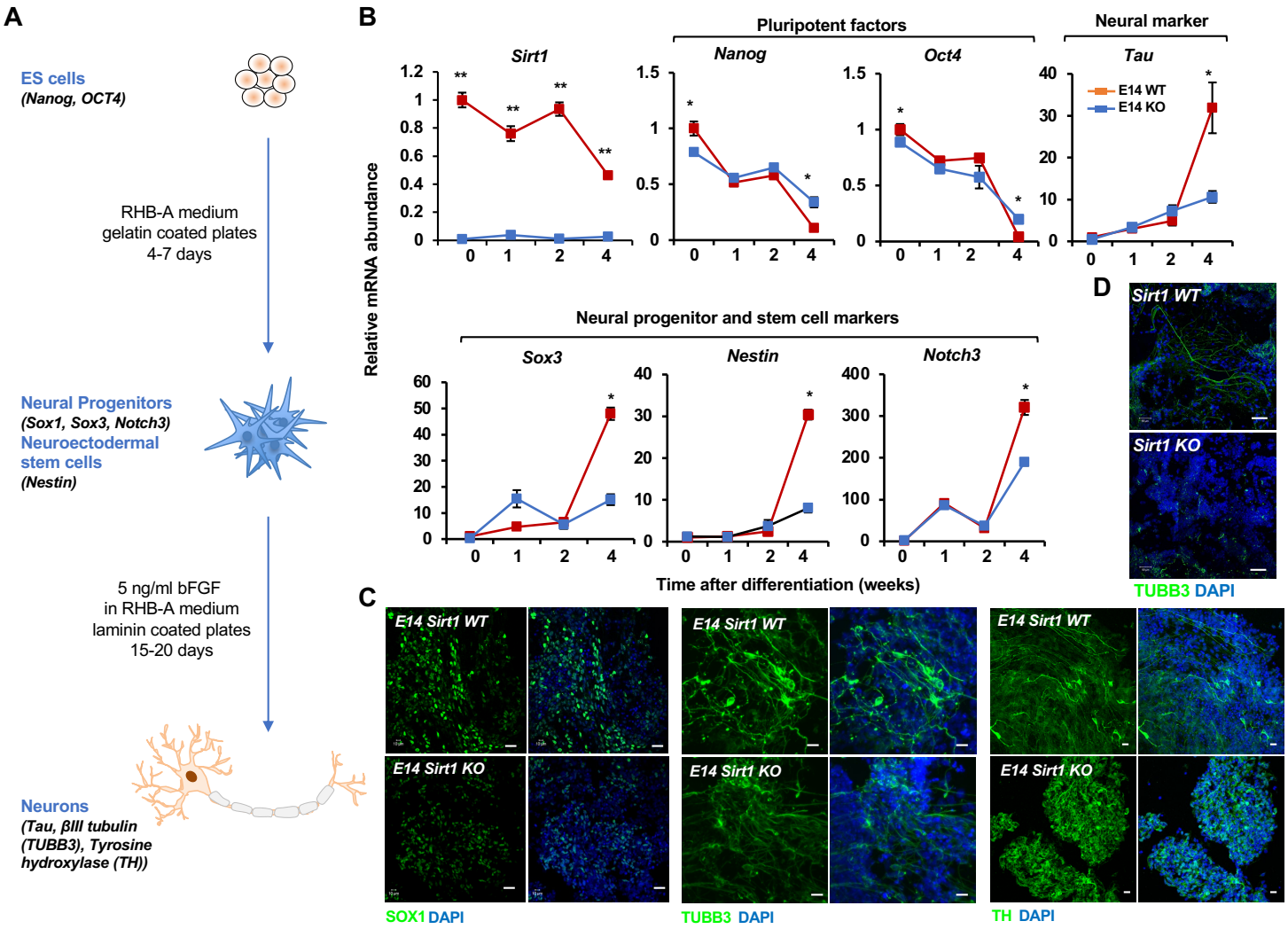

Figure 7. SIRT1 KO mESCs have an impaired neural differentiation in vitro.

(A) A diagram of the in vitro neural differentiation system. (B) SIRT1 KO E14 mESCs are less responsive to in vitro neural differentiation than WT mESCs. The expression of indicated genes were analyzed by qPCR during 4 weeks of in vitro neural differentiation. Please note that deletion of SIRT1 resulted in reduction in both repression of pluripotent factors and induction of markers for neural progenitors/stem cells and neurons (n=3 biological replicates, * p<0.05, **p<0.01). (C) SIRT1 KO E14 mESCs have reduced expression of neural differentiation markers and disordered neuronal morphology. WT and SIRT1 KO E14 mESCs after 4 weeks of in vitro neural differentiation were stained for a neural progenitor marker SOX1 (left panels) and neuronal markers □III tubulin (TUBB3, middle panels) and TH (right panels). Scale bars: 20μm. (D) SIRT1 KO mESCs have reduced expression of TUBB3 and mature neuronal morphology. WT and SIRT1 KO mESCs after 4 weeks of in vitro neural differentiation were stained for TUBB3. Scale bars: 20μm.

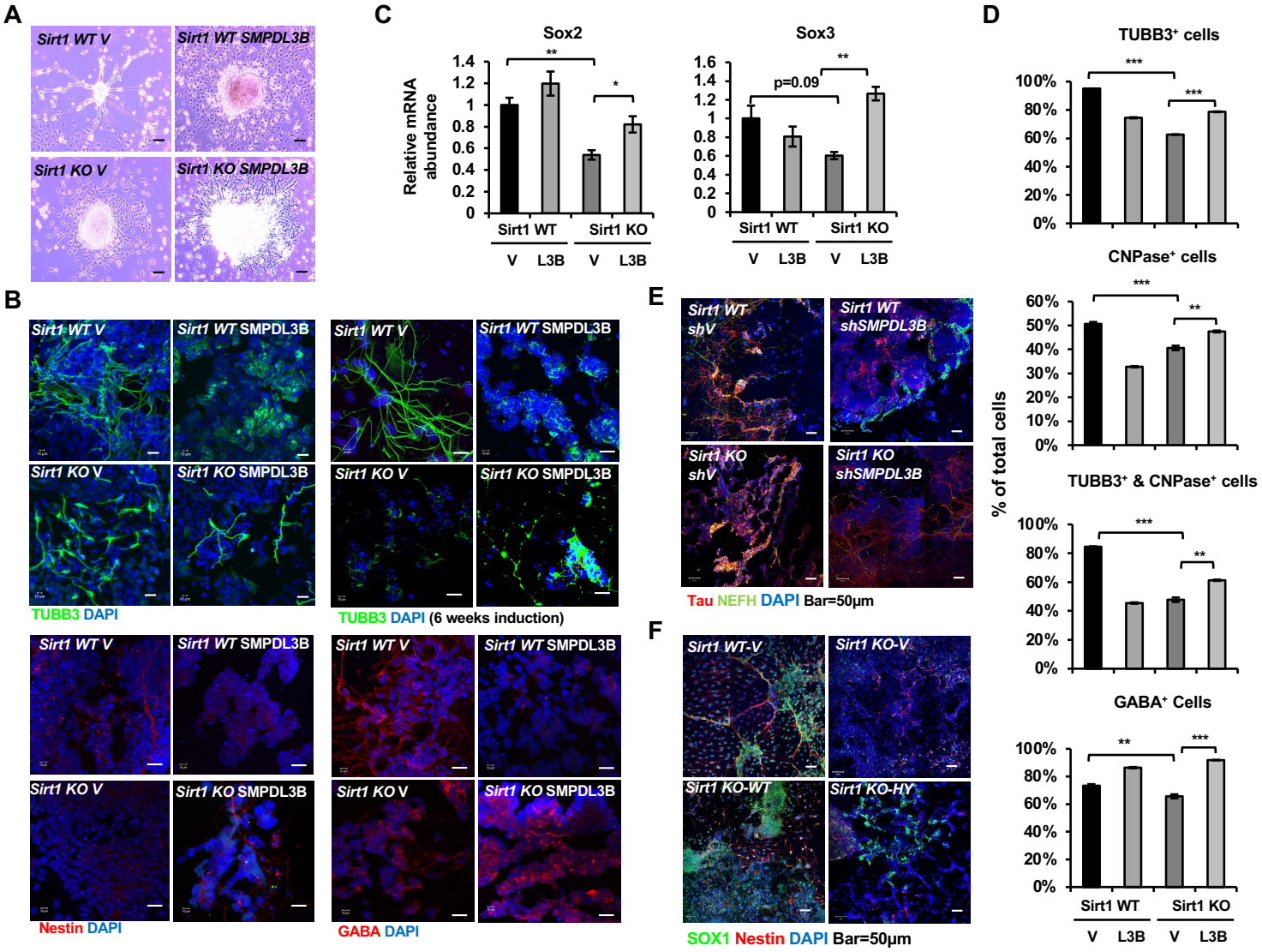

Figure 8. Reduced expression of SMPDL3B is partially responsible for impaired in vitro neural differentiation in SIRT1 KO mESCs.

(A) Overexpression of SMPDL3B partially rescues gross neuronal morphology in in vitro differentiated SIRT1 KO mESCs. WT and SIRT1 KO mESCs stably infected with lentiviral particles containing empty vector (V) or constructs expressing SMPDL3B protein were subjected to 4 weeks of in vitro neural differentiation. The cell morphology was analyzed using regular light microscopy fixed with ZEISS AxioCamHR camera. Scale bars: 20μm. (B) Overexpression of SMPDL3B partially rescues neuronal morphology in in vitro differentiated SIRT1 KO cells. WT and SIRT1 KO mESCs expressing vector (V) or SMPDL3B were differentiated as in (A). The expression of indicated markers and neuronal morphology were analyzed by immunofluorescence staining. Scale bars: 20μm. (C) Overexpression of SMPDL3B partially rescues the expression of neural progenitor markers in in vitro differentiated SIRT1 KO cells. WT and SIRT1 KO mESCs expressing vector (V) or SMPDL3B were differentiated as in (A). The expression of SOX2 and SOX3 were analyzed by qPCR (n=3 biological replicates, *p<0.05, **p<0.01). (D) Overexpression of SMPDL3B partially increased the fraction of differentiated cells in in vitro differentiated SIRT1 KO cells. WT and SIRT1 KO mESCs expressing vector (V) or SMPDL3B were differentiated as in (A). The fraction of differentiated cells positive of indicated neural markers were quantified by FACS (n=3 biological replicates, **p<0.01, ***p<0.001). (E) Knocking down SMPDL3B in WT mESCs impairs neural differentiation in vitro. WT and SIRT1 KO mESCs with or without stable knockdown of SMPDL3B were in vitro differentiated into neurons for 4 weeks. The expression of neural markers Tau and NEFH were analyzed by immunofluorescence staining. Scale bars: 50μm. (F) WT but not a catalytic inactive SIRT1 rescues neural differentiation in vitro. WT and SIRT1 KO mESCs expressing vector (V), WT SIRT1, or a mutant SIRT1 lacking catalytic activity (HY) were in vitro differentiated into neurons for 4 weeks. The expression of neural markers SOX1 and Nestin were analyzed by immunofluorescence staining. Scale bars: 50μm.

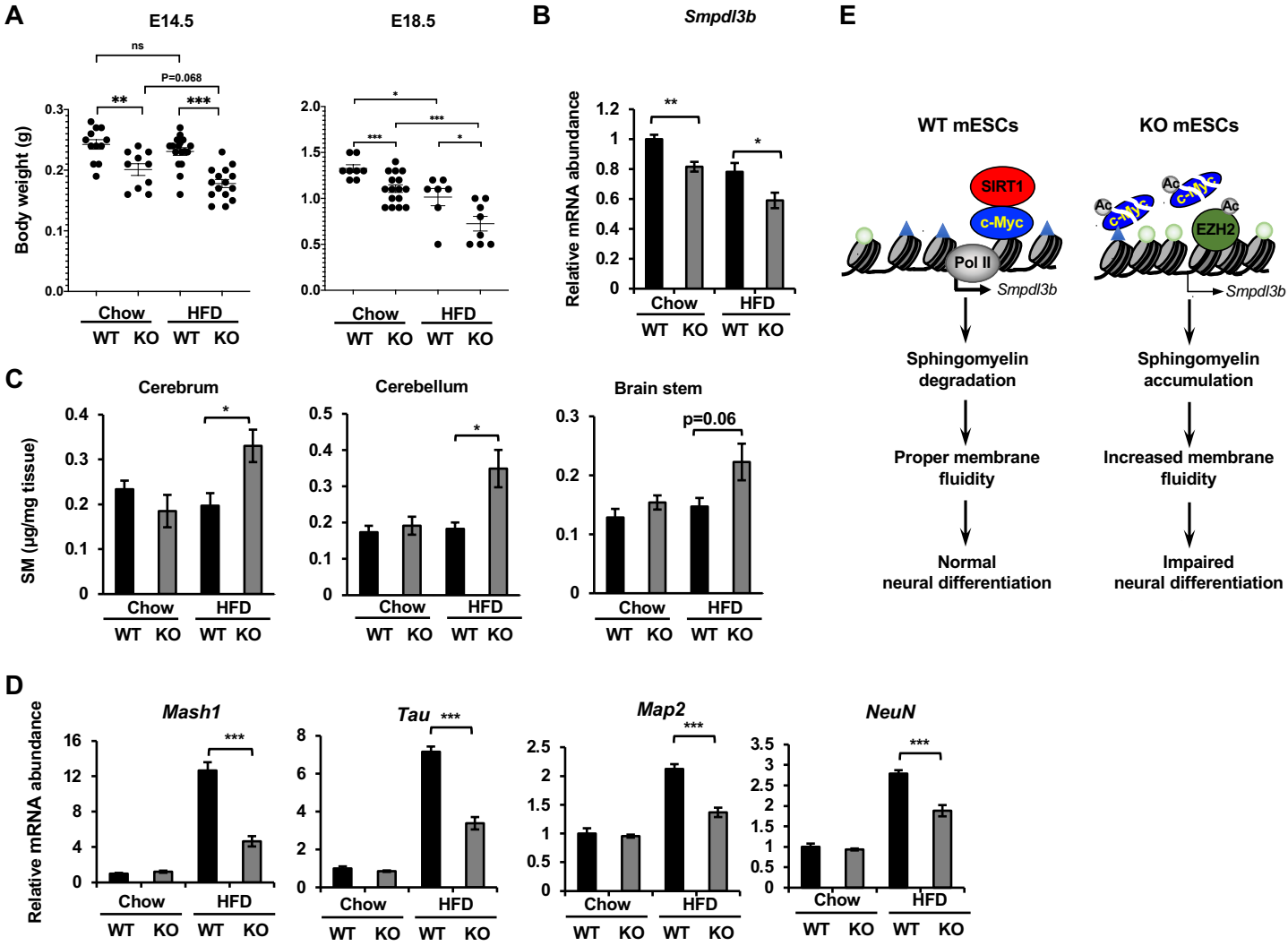

Figure 9. Maternal high-fat diet feeding impairs neural development in SIRT1 deficient embryos.

(A) Maternal high-fat diet feeding reduces body weight of embryos. Maternal high-fat diet (HFD) feeding was performed 3-4 weeks before pregnancy (pre-feeding) as described in Methods. Body weight of E14.5 and E18.5 embryos were measured (*p<0.05, **p<0.01, ***p<0.001). (B) SIRT1 KO embryos have reduced expression of Smpdl3b in brains. The mRNA levels of Smpdl3b in brain of E18.5 embryos from chow fed dams or HFD fed dams were analyzed by qPCR (n=6 embryos, *p<0.05, **p<0.01). (C) Maternal high-fat diet feeding induces sphingomyelin accumulation in brains of SIRT1 KO embryos. Maternal high-fat diet (HFD) feeding was performed 3-4 weeks before pregnancy (pre-feeding) as described in Methods. Brains from E18.5 embryos were dissected into three parts and the endogenous sphingomyelins were extracted and measured (n=6 embryos, *p<0.05). (D) Maternal high-fat diet feeding induces defective expression of neural markers in brains of SIRT1 KO embryos. The mRNA levels of indicated neural markers in brain of E18.5 embryos from chow fed dams or HFD fed dams were analyzed by qPCR (n=6 embryos, *p<0.05, **p<0.01, ***p<0.001). (E) SIRT1 regulates sphingomyelin degradation and neural differentiation of mESCs through c-Myc and EZH2. SIRT1 is highly expressed in mESCs cells, where it functions to promote association of c-Myc and recruitment of Pol II to activate transcription of Smpdl3b gene and subsequent sphingomyelin degradation. This action of SIRT1 is important for maintenance of a proper membrane fluidity for normal neural differentiation in response to nutritional/developmental cues. Deletion of SIRT1 causes hyperacetylation and instability of c-Myc, leading to Pol II depletion and transcriptional repression of Smpdl3b. SIRT1 deficiency induced hyperacetylation and stabilization of EZH2 likely enforce this transcriptional suppression by adding H3K27me3 mark. This transcriptional repression of Smpdl3b is associated with accumulation of sphingomyelin, which increases membrane fluidity and impairs neural differentiation. Light blue triangles: H3K4me3; Light green circles: H3K27me3; Ac: acetylation.

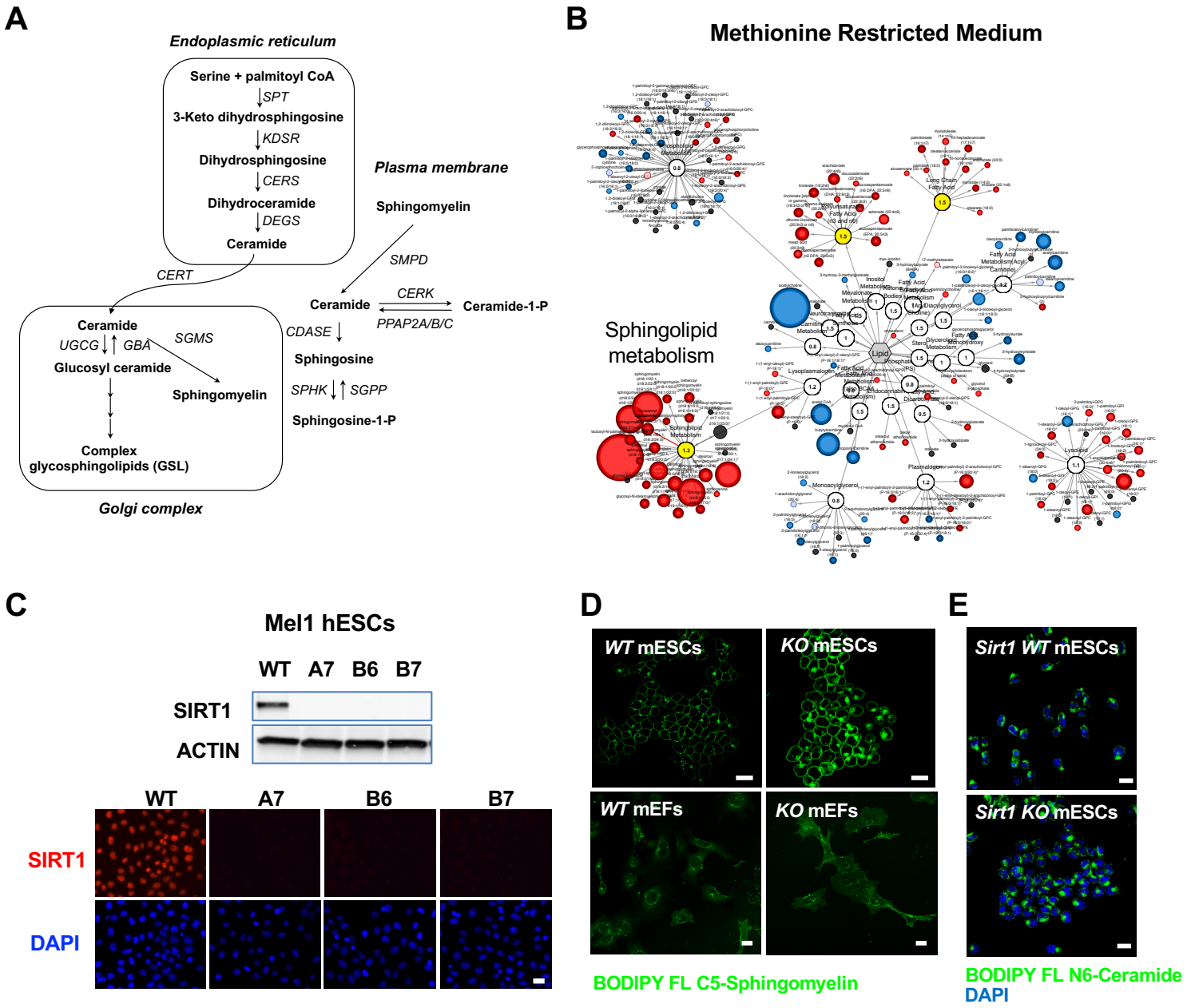

Figure S1. Deletion of SIRT1 in ESCs results in a dramatic accumulation of sphingomyelin.

(A) Key sphingolipid metabolic pathways (modified from [1]). SPT: serine palmitoyl transferase; KDSR: 3-keto dihydrosphingosine reductase; CERS, ceramide synthase; DEGS: dihydroceramide desaturase; CERT: ceramide transfer protein; UGCG: UDP-glucose ceramide glucosyltransferase; GBA: glucosyl ceramidase; SGMS: sphingomyelin synthase; SMPD: sphingomyelin phosphodiesterase; CERK: ceramide kinase; PPAP2A/B/C: phosphatidic acid phosphatase 2A/B/C; CDASE: ceramidase; SPHK: sphingosine kinase; SGPP: sphingosine-1-phosphate phosphatase. (B) Metabolomic analysis reveals a massive accumulation of sphingolipids in SIRT1 KO mESCs cultured in methionine restricted medium. WT and SIRT1 KO mESCs were cultured in a methionine restricted M10 medium containing 6 μM of methionine for 6 hours and metabolites were analyzed by metabolomics as described in Methods. The networks of significantly changed metabolites in lipid metabolism were analyzed by Cytoscape 2.8.3. Metabolites increased in SIRT1 KO mESCs were labeled red ($p<0.05$) or pink ($0.05<p<0.10$), metabolites decreased in SIRT1 KO mESCs were labeled blue ($p<0.05$) or light blue ($0.05<p<0.10$). Metabolite node size is proportional to the fold change in KO vs WT (n=5 biological replicates). (C) Deletion of SIRT1 in mel1 hESCs. SIRT1 KO hESCs were generated by crispr/Cas9 technology. The expression of SIRT1 protein was analyzed in three independent SIRT1 KO hESC lines by immuno-blotting (up) or immunofluorescent staining (bottom) with anti-SIRT1 antibodies. Bar, 20 μm. (D) Deletion of SIRT1 induces accumulation of sphingomyelin in mESCs but not in MEFs. Bars: 20μm. (E) SIRT1 KO mESCs have comparable levels of ceramide as WT mESCs. WT and SIRT1 KO mESCs were labeled with BODIPY FL- ceramide for 30 min at 4 ℃ then chased at 37 ℃ for 30 min. Bars: 20μm.

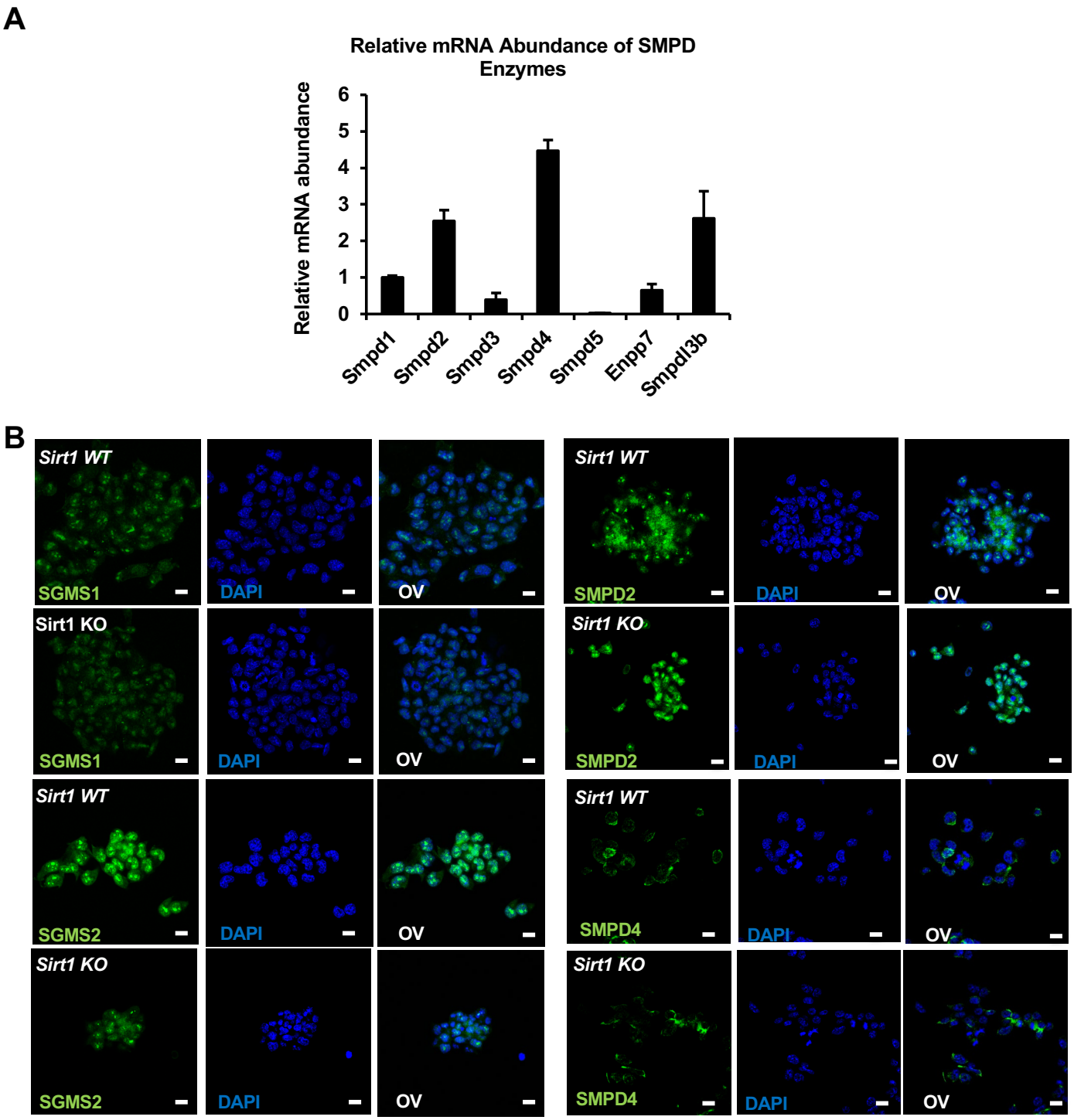

Figure S2. Expression of sphingolipid synthesis and degrading enzymes in WT and SIRT1 KO mESCs.

(A) *Smpdl3b* is one of the major *Smpds* in mESCs. The relative mRNA levels of indicated Smpds were measured by qPCR and normalized with standard curves using cDNA of each gene. Their relative abundance was then quantified and compared (n=3 biological replicates). (B) The expression of SGMS1, SGMS2, SMPD2, and SMPD4 in WT and SIRT1 KO mESCs were analyzed by immunofluorescence staining. Bars: 20μm.

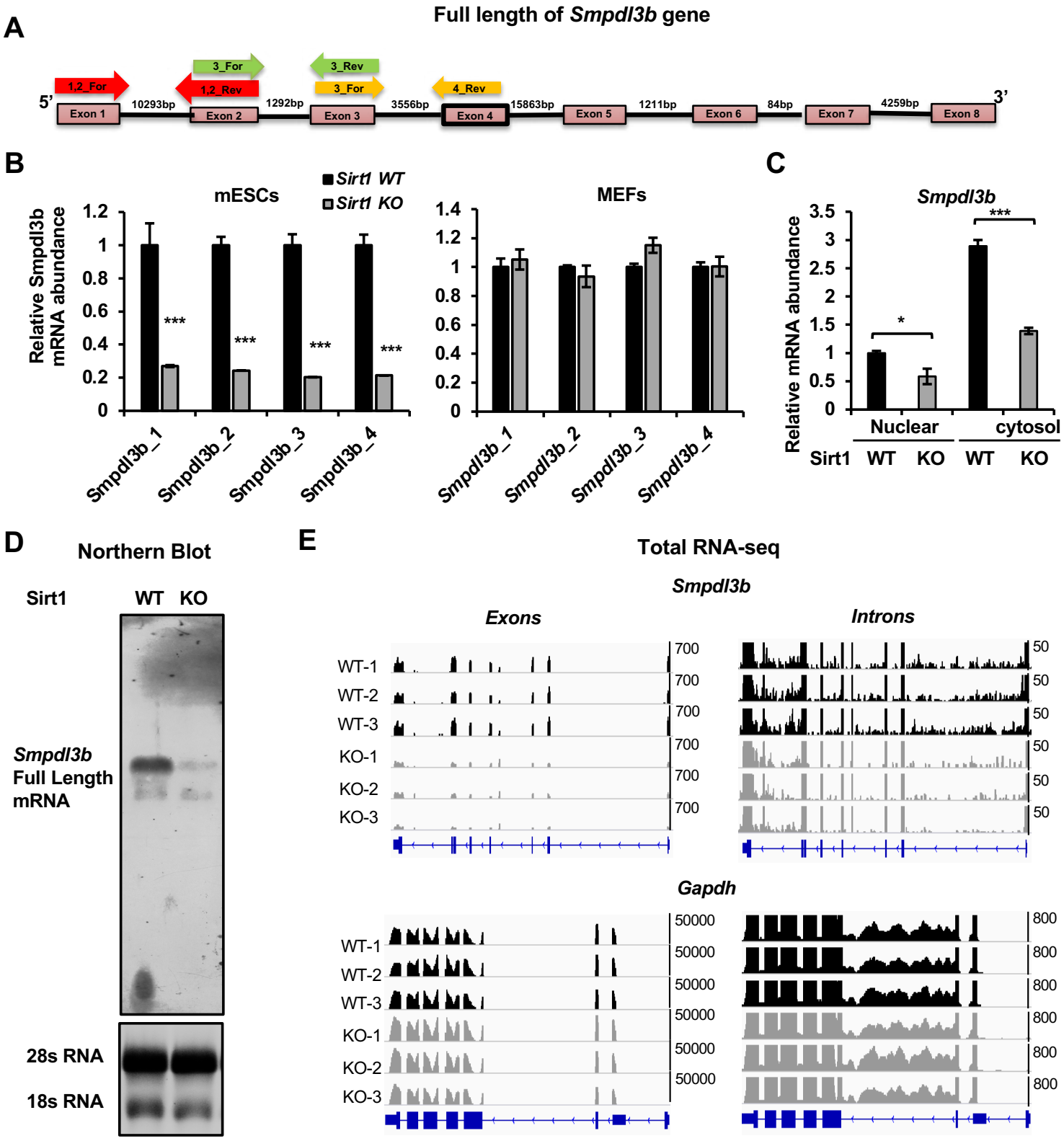

Figure S3. Deletion of SIRT1 reduces transcription of *Smpdl3b* gene.

(A) Diagram of mouse *Smpdl3b* gene structure. The locations of indicated qPCR primers were denoted. (B) SIRT1 KO mESCs but not MEFs have reduced mature *Smpdl3b* mRNA. The relative mature mRNA levels of Smpdl3b were analyzed by qPCR by four different pairs of primers as indicated in (A) (n=3 biological replicates, ***p<0.001). (C) SIRT1 KO mESCs have reduced *Smpdl3b* mRNA in both nuclear and cytosol. The nuclear and cytosol fraction of WT and SIRT1 KO mESCs were separated as described in Methods and mRNA levels of *Smpdl3b* were analyzed by qPCR (n=3 biological replicates, *p<0.05, ***p<0.001). (D) SIRT1 KO mESCs have reduced levels of full length *Smpdl3b* mRNA. Total RNA from WT and SIRT1 KO mESCs were probed for full length *Smpdl3b* mRNA by Northern blotting as described in Methods. (E) SIRT1 KO mESCs have reduced abundance of transcripts of *Smpdl3b* gene at both intronic and exonic regions. Ribo-minus total RNA from WT and SIRT1 KO mESCs were sequenced by Nova-seq. The total reads mapped to the whole mouse Smpdl3b gene were shown. The transcript abundance of *Gapdh* gene at both exonic and intronic regions was shown as control.

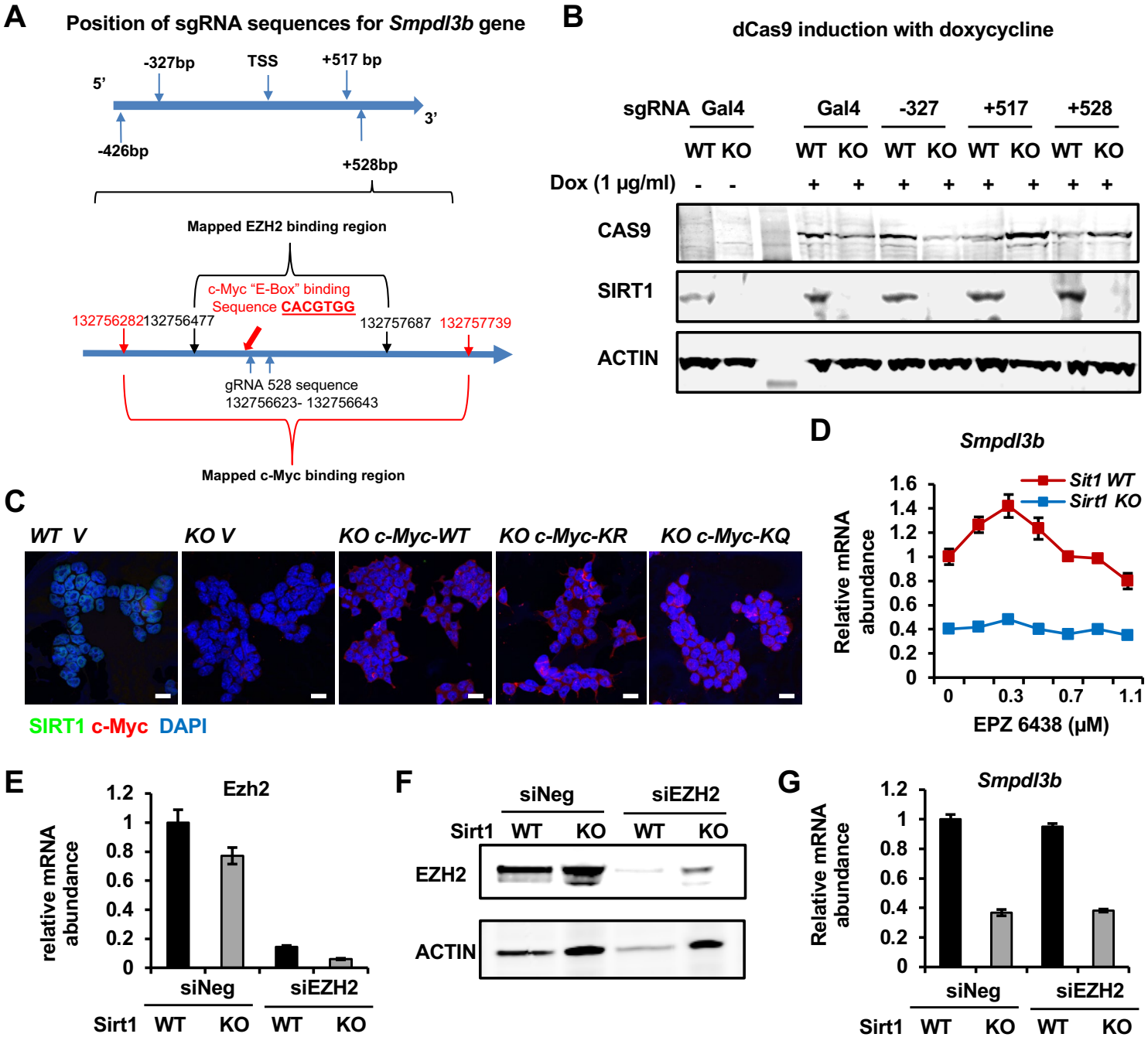

Figure S4. SIRT1 promotes the transcription of *Smpdl3b* through c-Myc but not EZH2 in mESCs.

(A) The positions of gRNA targeting sequences on the *Smpdl3b* gene. The targeting sequence of gRNA +528 is located in a region containing both mapped c-Myc binding site and EZH2 binding site. (B) The expression of dCas9 and SIRT1 in WT and SIRT1 KO dCas9 mESCs. WT and SIRT1 KO dCas9 mESCs transfected with indicated sgRNA were treated with 1 μg/ml Dox for 48 hours. (C) Overexpression of WT, K323R, and K323Q mutant of c-Myc in SIRT1 KO mESCs. WT and SIRT1 KO mESCs were infected with lentiviral particles containing empty vector (V) or constructs expressing WT, K323R (KR), or K323Q (KQ) mutant of c-Myc. Bars: 20μm. (D) Inhibition of EZH2 have limited effect on the expression of *Smpdl3b* gene in mESCs. WT and SIRT1 KO mESCs were treated with EPZ6438 at indicated concentrations for 48 hours (n=3 biological replicates). (E-F) Knocking down EZH2 in mESCs. WT and SIRT1 KO mESCs were transfected with control siRNA (siNeg) or siRNAs against EZH2 (siEZH2) for 48 hours. The expression of *Smpdl3b* was analyzed by (E) qPCR (n=3 biological replicates) and (F) immunoblotting. (G) Knocking down EZH2 have minimal effect on the expression of *Smpdl3b* gene in mESCs (n=3 biological replicates).

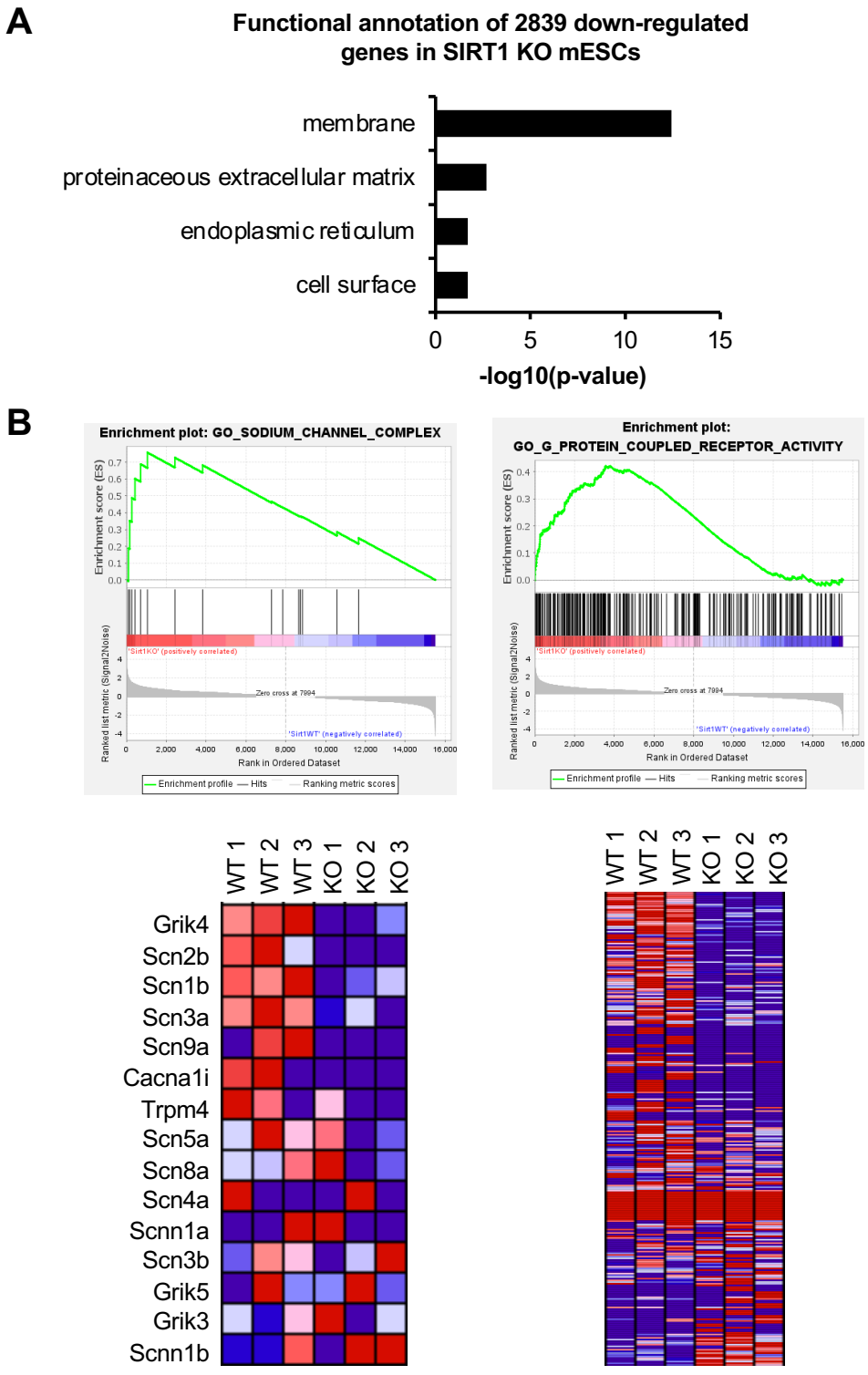

Figure S5. SIRT1 deficiency in mESCs significantly reduces the expression of genes involved in membrane signaling.

(A) Genes involved in membrane function are significantly enriched in genes downregulated in SIRT1 KO mESCs. (B) Two major impaired membrane pathways in SIRT1 KO mESCs. GSEA analysis of transcriptomes from WT and SIRT1 KO mESCs was performed as described in Methods. Two major downregulated membrane pathways were shown (n=3 biological replicates).